



UNIVERSITY OF GRONINGEN

MASTER THESIS

---

# (Quantum) Spin Hall Effect in electron and hole systems

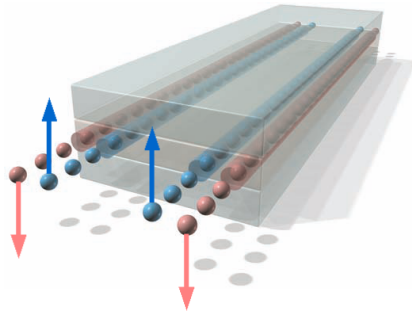
---

*Author:*

Alina M. HRISCU

*Supervisor:*

Maxim V. MOSTOVOY



INSTITUTE FOR THEORETICAL PHYSICS  
ZERNIKE INSTITUTE FOR ADVANCED MATERIALS

August 7, 2008



# Contents

<b>1</b>	<b>Introduction</b>	<b>5</b>
1.1	Motivation . . . . .	5
1.2	Classical Hall effect . . . . .	6
1.3	Quantum Hall effect . . . . .	8
1.3.1	Edge states . . . . .	11
<b>2</b>	<b>Intrinsic spin-Hall effect in 2D electron gases</b>	<b>16</b>
2.1	Introduction . . . . .	16
2.2	Rashba Hamiltonian . . . . .	17
2.3	A two-dimensional electron gas in a perpendicular electric field	18
2.4	Landau-Lifshitz equation . . . . .	19
2.5	Calculation of the spin current and spin resistivity . . . . .	22
2.6	Further remarks and conclusions . . . . .	24
<b>3</b>	<b>Spin-Hall effect in hole-doped semiconductors</b>	<b>26</b>
3.1	Introduction . . . . .	26
3.2	$\mathbf{k} \cdot \mathbf{p}$ approximation and Luttinger model . . . . .	27
3.3	Introducing an electric field in the Luttinger Hamiltonian . . . . .	29
3.4	Abelian approximation . . . . .	33
3.5	Non-Abelian spin current . . . . .	36
3.6	Spin current obtained from conservation of the total angular momentum . . . . .	37
3.7	Further remarks and conclusions . . . . .	38

<b>4</b>	<b>Quantum spin Hall effect in semiconductor quantum wells</b>	<b>39</b>
4.1	Introduction . . . . .	39
4.2	Effective model for the quantum spin-Hall state in HgTe/CdTe quantum wells . . . . .	41
4.3	Conclusions . . . . .	45
<b>A</b>	<b><math>k \cdot p</math> approximation for semiconductors</b>	<b>49</b>
<b>B</b>	<b>Integrating the equation of motions for holes in the Abelian approximation</b>	<b>52</b>
<b>C</b>	<b>Acknowledgements</b>	<b>54</b>

# Chapter 1

## Introduction

This thesis could have been organized in two very different parts. That is because for the first part of my research year I have looked at a completely different topic than this thesis is about (frustrated spin chains was the other topic). Instead of having a rather lengthy thesis about two such different subjects, I have decided to write just about the fascinating spin-Hall effect.

Much like graphene (which was also in my list of subjects on which I wanted to do my Master project on), the quantum spin-Hall effect is a “hot topic” which has attracted a great deal of interest from the scientific community. This is mainly because of promising spintronics applications, but also because it poses fundamental questions about a new phase of matter. It all started with the spin-Hall effect, without “quantum” attached to it. In this case the spin-resistivity is not quantized, but it has an universal value.

In this thesis the chronological order of these topics will be preserved. In the introductory chapter a brief review of the classical and quantum Hall effect is given. The first chapter deals with the spin-Hall effect in two-dimensional electron gases. Chapter 3 is about the same effect, but in three-dimensional p-doped semiconductors. Although the mathematical approach is different, the physical origin of the spin-Hall effect is similar to the one discussed in chapter 2. The last chapter of the thesis aims to give a brief overview of the quantum spin-Hall effect and its physical origin.

### 1.1 Motivation

The possibility to manipulate the spin degree of freedom of electron (spintronics) has raised a lot of interest in the scientific world for the past 20

years. Apart from many potential applications in information technology it also poses many interesting and challenging fundamental questions.

In the electronic circuits, on which our present technology is based, dissipation of the charge currents induces an intrinsic limitation. On the other hand, in two-dimensional semiconductors showing quantum Hall effect (QHE), the electrical current is flowing without dissipation. Unfortunately, the experimental conditions necessary to reach the quantum Hall effect (magnetic fields of order of 10 T and extremely low temperatures) make these systems impractical. Similarly, the dissipationless transport of charge in superconductors only becomes possible at rather low temperatures.

The (quantum) spin Hall effect may help to overcome these limitations. It is the generalization of the quantum Hall effect for spin systems. The spin Hall effect occurs in paramagnets with strong spin-orbit coupling. A spin current perpendicular to a charge current is generated in the absence of magnetic field. This leads to a spin accumulation on the edges of the sample. While the charge current necessary to separate spins is dissipative, the spin current is dissipationless and has a universal (quantized) conductance.

There are several theoretical models used to calculate the spin currents and the corresponding resistivity. The main difference between them is the phenomenological form of the spin-orbit coupling. Murakami et al. [1] predicted the effect in p-doped semiconductors with Luttinger type of spin-orbit, while Sinova et al.[2] used Rashba spin-orbit coupling in n-doped semiconductors.

Remarkably, recent experiments provide a strong evidence for the existence of the quantum spin Hall effect [3]. The spin-Hall effect is a non-trivial consequence of first-principles physics. The quantum spin-Hall effect represents a topologically distinct new state of matter.

## 1.2 Classical Hall effect

The Hall effect is named after Edwin H. Hall who discovered this novel phenomenon in 1879. If an electric current flows through a conductor in a magnetic field, the magnetic field exerts a transverse force on the moving charge carriers which tends to push them to one side of the conductor. This is most evident in a thin flat conductor as pictured in Fig. 1.2. A buildup of charge at the sides of the conductors will balance this magnetic influence, producing a measurable voltage between the two sides of the conductor. The presence of this measurable transverse voltage is called the Hall effect.

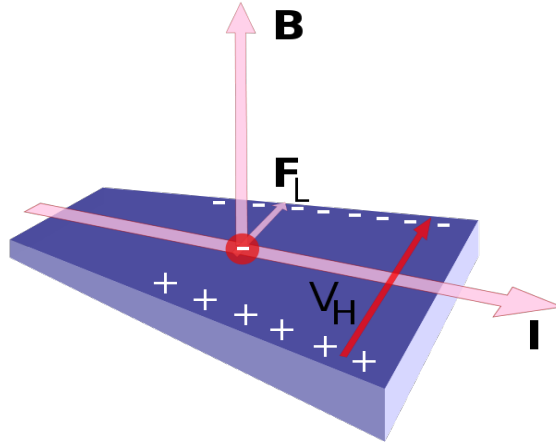


Figure 1.1: By applying an electric field and a perpendicular magnetic field, a potential difference (Hall voltage) appears between the sample edges. The Hall voltage arises because the electrons and holes are deflected by the magnetic field.

The Hall coefficient is defined as  $R_H = V_H/I$ , the Hall voltage over the current in the direction of the electric field. For a simple metal where there is only one type of charge carrier (electrons) the Hall voltage is given by

$$V_H = \frac{-IB/d}{ne}, \quad (1.1)$$

where  $I$  is the current across the plate length,  $B$  is the magnetic flux density,  $d$  is the thickness of the plate,  $e$  is the electron charge, and  $n$  is the charge carrier density of the carrier electrons. Then the Hall coefficient is expressed as

$$R_H = \frac{E_y}{j_x B} = \frac{V_H}{IB/d} = -\frac{1}{ne}. \quad (1.2)$$

As a result, the Hall effect is very useful as a mean to measure both the carrier density and the magnetic field, as well as the sign of the charge carriers.

One very important feature of the Hall effect is that it differentiates between positive charges moving in one direction and negative charges moving in the opposite. The Hall effect offered the first real proof that electric currents in metals are carried by moving electrons, not by protons.

### 1.3 Quantum Hall effect

The quantum Hall effect is one of the most remarkable condensed-matter phenomena discovered in the second half of the 20th century. It rivals superconductivity in its fundamental significance as a manifestation of quantum mechanics on macroscopic scales. It occurs in the same geometry as the classical Hall effect, but in very thin samples (two-dimensional electron gas) subject to a strong magnetic field. The basic experimental observation is the nearly vanishing dissipation

$$\sigma_{xx} \rightarrow 0 \tag{1.3}$$

and the quantization of the Hall resistance

$$R_H = \frac{1}{\nu} \frac{h}{e^2} \tag{1.4}$$

of a real (as opposed to some theorists fantasy) transistor-like device (similar in some cases to the transistors in computer chips). In sufficiently pure samples, this quantization is universal and independent of all microscopic details such as the type of semiconductor material, the precise value of the magnetic field, and so forth. As a result, the effect is now used to maintain the standard of electrical resistance by metrology laboratories around the world. In addition, since the speed of light is now defined, a measurement of  $e^2/h$  is equivalent to a measurement of the fine structure constant of fundamental importance in quantum electrodynamics.

The quantum Hall effect is a topic by itself, which can be discussed extensively. There are books just about it. A complete treatment implies broken symmetries, novel states of matter, Skyrmions, as well as fractional quantum Hall effect, anomalous Hall effect. In this section we limit ourselves to the integer quantum Hall effect.

The integer quantum Hall effect can be understood in both classical and semiclassical pictures as well as in a full-quantum mechanical approach. In this section we will mention the quantum mechanical justification of the effect. The edge states mechanism will also be addressed, because of its importance for the quantum spin-Hall effect.

In the so-called integer quantum Hall effect discovered by von Klitzing in 1980 [4], the quantum number  $\nu$  is a simple integer with a precision of about  $10^{-10}$  and an absolute accuracy of about  $10^{-8}$  (both being limited by our ability to do resistance metrology).



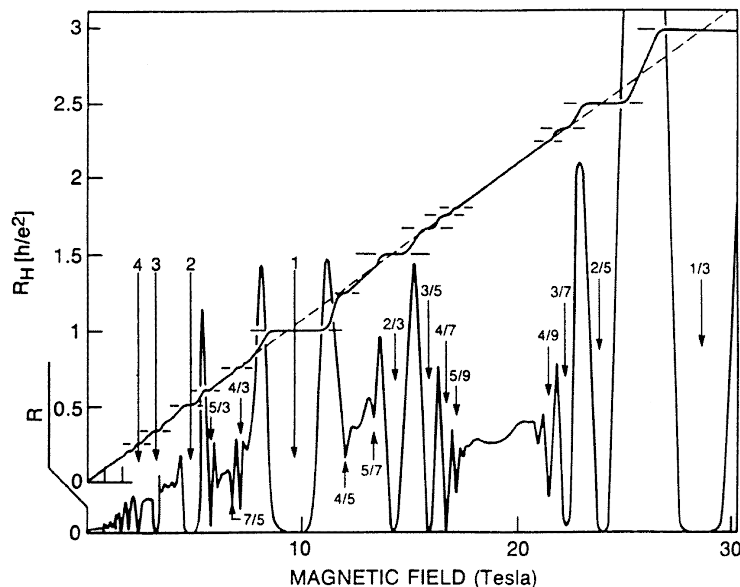


Figure 1.2: Integer and fractional quantum Hall transport data showing the plateau regions in the Hall resistance  $R_H$  and associated dips in the dissipative resistance  $R$ . The numbers indicate the Landau level filling factors at which various features occur.

In 1982, Tsui, Störmer and Gossard [5] discovered that in certain devices with reduced (but still non-zero) disorder, the quantum number could take on rational fractional values. This so-called fractional quantum Hall effect is the result of quite different underlying physics involving strong Coulomb interactions and correlations among the electrons. The particles condense into special quantum states whose excitations have the bizarre property of being described by fractional quantum numbers, including fractional charge and fractional statistics that are intermediate between ordinary Bose and Fermi statistics. The fractional quantum Hall effect has proven to be a rich and surprising arena for the testing of our understanding of strongly correlated quantum systems.

Now we move on to see what happens when electrons are confined to a two-dimensional space in high magnetic field. We will of course get a certain discrete set of allowed energy levels (the so-called Landau levels), like ones for the hydrogen atom. We begin by writing the Hamiltonian of the system:

$$H_0 = \frac{1}{2m^*} \sum_j \left[ \mathbf{p}_j + e\mathbf{A}(\mathbf{r}_j) \right]^2 \quad (1.5)$$

Here,  $\mathbf{A}(\mathbf{r}_j)$  is the vector potential at the position  $\mathbf{r}_j$  of the  $j$ th electron,  $\mathbf{p}_j$  its momentum and  $m^*$  its effective (band) mass. In the absence of potentials that break the translational invariance along the  $x$  axis, and using the Landau gauge,

$$\mathbf{A}(\mathbf{r}) = xB\hat{y}, \text{ with } \nabla \times \mathbf{A} = B\hat{z}, \quad (1.6)$$

we can write the single particle states as:

$$\Psi_{kn}(x, y) = \Phi_{kn}(y)e^{ikx}, \quad (1.7)$$

where the indices  $k$  and  $n$  are used to number the state, and  $k$  is the momentum along the  $x$  axis. Then we can use periodic boundary conditions along the  $x$  direction and get the allowed values for  $k$ , namely  $2\pi m$ , with  $m$  integer and  $L_x$  the length along the  $x$  axis.

By applying the Hamiltonian (1.5) to the above wavefunction, we obtain a single-particle Schrödinger equation that we can write, for each allowed value of  $k$ , as the equation for a harmonic oscillator centered at

$$y_k = -l_B^2 k, \quad (1.8)$$

with  $l_B = \sqrt{\frac{\hbar}{eB}}$  the magnetic length.

The energy eigenvalues will be:

$$\epsilon_{nk} = \hbar\omega_c \left( n + \frac{1}{2} \right), n = 0, 1, 2, \dots \quad (1.9)$$

where  $\omega_c = \frac{eB}{m^*}$  is the cyclotron frequency. They do not depend on  $k$ . For each  $n$ , this gives us a Landau level and there is a huge number of  $k$  states that have the same energy  $\epsilon_{nk}$ . Its easy to show that each Landau level contains a number of states  $d$ , given by:

$$d = \frac{L_x L_y}{2\pi l_B^2}, \quad (1.10)$$

which is called the degeneracy of a level.  $D = \frac{d}{L_x L_y}$  is therefore the degeneracy per unit area. It should not be surprising that  $D$  is proportional to  $B$ , because from the classical perspective, higher magnetic field means smaller radius of the electrons orbits and so, more orbits can fit in a given area without overlapping (hence higher degeneracy). Dividing  $N$  by  $D$  defines the filling factor  $\nu$ . This tells us how many Landau levels are occupied. At very high magnetic field,  $D$  is way larger than  $N$  and all the electrons lie in the lowest Landau level ( $\nu < 1$ ). On reducing  $B$ , the spacing between the levels,  $\omega_c$ ,

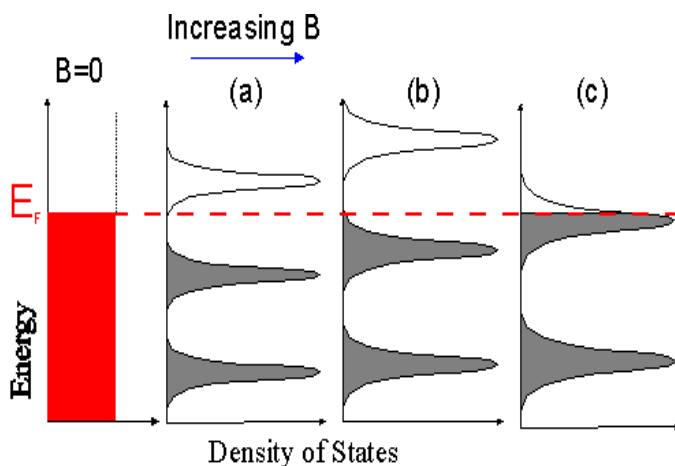


Figure 1.3: The Landau bands as a function of magnetic field. The values of resistivity depend of where the Fermi level (red online) lies, as explained in the text.

as well as their degeneracy, decreases. We will at some point reach a critical value of the magnetic field (lets call it  $B_1$ ), for which  $D = N$  and the first Landau level is fully occupied. Further reduction forces the electrons up into the second Landau level and then we will reach a field  $B_2$ , for which  $\nu = 2$  and so on (see Fig.(1.3)).

Now we can express the Hall resistance  $R_H$  as  $\frac{h}{e^2\nu}$ . At the critical values of the magnetic field that we discussed above,  $\nu$  will be an integer. This explains the integer plateaux.

One would expect the plateaux to be infinitely narrow. The reason why this is not the case is disorder. In the presence of impurities, the many independent quantum states that make up a given Landau level are no longer precisely equal in energy. Thus the Landau levels split and turn into energy bands made up of many distinct levels. Upon changing the magnetic field when the Fermi level lies in one of these Landau bands, the resistivity doesn't change. This explains the finite width of the plateaux.

### 1.3.1 Edge states

Let us now consider the case of a uniform electric field pointing in the  $y$  direction and giving rise to the potential energy

$$V(r) = +eEy. \quad (1.11)$$

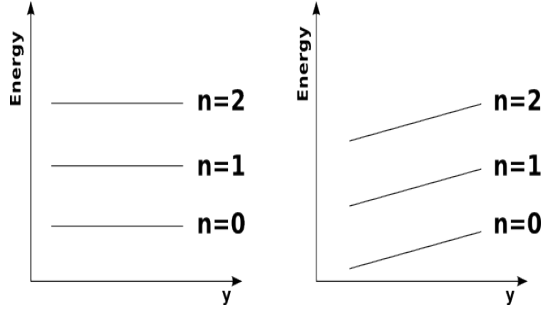


Figure 1.4: Illustration of electron Landau energy levels  $(n + 1/2)\hbar\omega_c$  vs. position  $y_k = kl_B^2$ . (a) For zero electric field (a) and (b) for nonzero electric field in the  $+y$  direction.

This potential still has translation symmetry in the  $x$  direction and so the Landau gauge choice is still the most convenient. Again separating variables we see that the solution of the Schrödinger equation is nearly the same as before, except that the displacement of the harmonic oscillator is slightly different. The new Hamiltonian is just the old one, Eq.(1.5), with the addition of

$$\sum_j eEy_j \quad (1.12)$$

Completing the square we see that the oscillator is now centered at the new position

$$Y_k = -l_B^2 k - \frac{eE}{m\omega_c^2}, \quad (1.13)$$

and the energy eigenvalue is now linearly dependent on  $Y_k$  (and therefore linear in the  $k$  momentum)

$$\epsilon_k = \frac{1}{2}\hbar\omega_c + eEY_k + \frac{1}{2}m\bar{v}^2, \quad (1.14)$$

where  $\bar{v} \equiv \frac{E}{B}$ . It should be noted that the applied electric field tilts the Landau levels in the sense that their energy is now linear in position as illustrated in Fig.(1.3.1). This means that there are degeneracies between different Landau level states because different kinetic energy can compensate different potential energy in the electric field. Nevertheless, we have found the exact eigenstates (i.e., the stationary states). It is not possible for an electron to decay into one of the other degenerate states because they have different canonical momenta.

Now we can consider the problem of electrons confined in a Hall bar of finite width by a non-uniform electric field. For simplicity, we will consider the

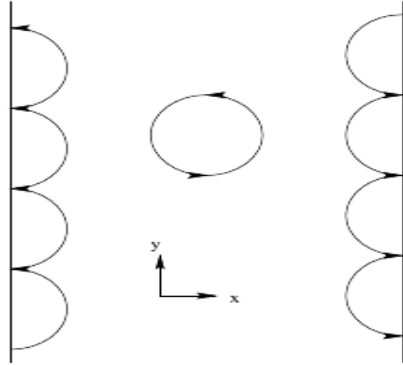


Figure 1.5: Semi-classical view of skipping orbits at the Fermi level at the two edges of the sample where the confining electric field causes  $E \times B$  drift. The circular orbit illustrated in the center of the sample carries no net drift current if the local electric field is zero.

situation where the potential  $V(y)$  is smooth on the scale of the magnetic length, but this is not central to the discussion. If we assume that the system still has translation symmetry in the  $x$  direction, the solution to the Schrödinger equation must still be of the form

$$\Psi_{kn}(x, y) = \Phi_{kn}(y)e^{ikx}. \quad (1.15)$$

The function  $\Phi_{kn}(y)$  will no longer be a simple wave function of harmonic oscillator as we found in the case of the uniform electric field. However we can anticipate that  $\Phi_{kn}(y)$  will still be peaked near (but in general not precisely at) the point  $Y_k k l_B^2$ . The eigenvalues  $\epsilon_k$  will no longer be precisely linear in  $k$  but will still reflect the kinetic energy of the cyclotron motion plus the local potential energy  $V(Y_k)$ . We see that the group velocity

$$\mathbf{v}_k = \frac{1}{\hbar} \frac{\partial \epsilon_k}{\partial k} \hat{x} \quad (1.16)$$

has the opposite sign on the two edges of the sample. This means that in the ground state there are edge currents of opposite sign flowing in the sample. The semi-classical interpretation of these currents is that they represent skipping orbits in which the circular cyclotron motion is interrupted by collisions with the walls at the edges, as illustrated in Fig.(1.3.1).

One way to analyze the Hall effect in this system is quite analogous to the Landauer picture of transport in narrow wires [6]. The edge states play the role of the left and right moving states at the two Fermi points. Because

(as we saw earlier) momentum in a magnetic field corresponds to position, the edge states are essentially real space realizations of the Fermi surface. A Hall voltage drop across the sample in the  $x$  direction corresponds to a difference in electrochemical potential between the two edges. Borrowing from the Landauer formulation of transport, we will choose to apply this in the form of a chemical potential difference and ignore any changes in electrostatic potential. What this does is increase the number of electrons in skipping orbits on one edge of the sample and/or decrease the number on the other edge. Previously the net current due to the two edges was zero, but now there is a net Hall current. To calculate this current we have to add up the group velocities of all the occupied states

$$I = -\frac{e}{L_y} \int_{-\infty}^{+\infty} dk \frac{L_y}{2\pi} \frac{1}{\hbar} \frac{\partial \epsilon_k}{\partial k} n_k, \quad (1.17)$$

where for the moment we assume that in the bulk, only a single Landau level is occupied and  $n_k$  is the probability that state  $k$  in that Landau level is occupied. Assuming zero temperature and noting that the integrand is a perfect derivative, we have

$$I = -\frac{e}{h} \int_{\mu_R}^{\mu_L} d\epsilon = -\frac{e}{h} [\mu_L - \mu_R] \quad (1.18)$$

(To understand the order of limits of integration, recall that as  $k$  increases,  $Y_k$  decreases.) The definition of the Hall voltage drop is

$$(+e)V_H \equiv (+e)[V_R - V_L] = [\mu_R - \mu_L] \quad (1.19)$$

Hence

$$I = \nu \frac{e^2}{h} V_H, \quad (1.20)$$

where we have now allowed for the possibility that  $\nu$  different Landau levels are occupied in the bulk and hence there are separate edge channels contributing to the current. This is the analog of having  $\nu$  open channels in the Landauer transport picture. In the Landauer picture for an ordinary wire, we are considering the longitudinal voltage drop (and computing  $\sigma_{xx}$ ), while here we have the Hall voltage drop (and are computing  $\sigma_{xy}$ ). The analogy is quite precise however because we view the right and left movers as having distributions controlled by separate chemical potentials. It just happens in the quantum Hall effect case that the right and left movers are physically separated in such a way that the voltage drop is transverse to the current.

Using the above result and the fact that the current flows at right angles to the voltage drop we have the desired results

$$\sigma_{xx} = 0 \tag{1.21}$$

$$\sigma_{xy} = -\nu \frac{e^2}{h}, \tag{1.22}$$

with the quantum number  $\nu$  being an integer. This is because no other states of the same energy are available. If the disorder causes Landau level mixing at the edges to occur (because the confining potential is relatively steep) then it is possible for an electron in one edge channel to scatter into another, but the current is still going in the same direction so that there is no reduction in overall transmission probability. It is this chiral (unidirectional) nature of the edge states which is responsible for the fact that the Hall conductance is correctly quantized independent of the disorder.

In Chapter (4), dealing with quantum spin-Hall effect, we will see that inverted-gap semiconductor heterostructures in electric field exhibit chiral edge channels, similar to the ones discussed above for the quantum Hall effect. For the quantum spin-Hall effect these edge channels carry spin current instead of charge current, are responsible for the quantization of the spin current as well as being resistant against disorder.

# Chapter 2

## Intrinsic spin-Hall effect in 2D electron gases

### 2.1 Introduction

The spin Hall effect is the generation in a paramagnetic system of a spin current perpendicular to an applied charge current leading to spin accumulations with opposite magnetization at the edges. This effect was first predicted more than three decades ago by invoking the phenomenology of the earlier theories of the anomalous Hall effect in ferromagnets, which associated its origin with asymmetric Mott-skew and side-jump scattering from impurities due to spin-orbit coupling [7, 8].

Recently, the possibility of an intrinsic (dependent only on the electronic structure) spin-Hall effect has been put forward [2] and [1] predicting the presence of a spin current generated perpendicular to an applied electric field in semiconducting systems with strong spin-orbit coupling, and impurity scattering playing a minor role. This proposal has generated an extensive theoretical debate in a very short time motivated by its novel physical concept and potential as a spin injection tool. The interest has also been dramatically enhanced by experiments by two groups reporting the first observations of the spin-Hall effect in n-doped semiconductors [9] and [10] and in 2D hole gases [11].

These experiments measure directly the spin accumulation induced at the edges of the examples through different optical techniques. On the other hand, most of the early theory has focused on the spin-current generated by an electric field, which would drive such spin-accumulation. In most



studies this spin current and its associated conductivity has been defined as  $j_y^z = \{v_y, S_z\}/2 = \sigma^{SHE} E_x$ . This choice is natural but not unique, since in the presence of spin-orbit coupling there is no continuity equation for spin density as is the case for charge density. The actual connection between the spin-accumulation and the induced spin-current is not straightforward in the situations where spin-orbit coupling is strong and this relation is the focus of current research and one of the key challenges ahead.

In this chapter (based on the seminal paper of Sinova et.al [2]) we will present in detail the calculation of the spin current and spin resistivity. The structure is as follows : we start from an intuitive derivation of the Rashba spin-orbit coupling Hamiltonian, and then we derive the spin-dynamics equation (Landau-Lifshitz equation) in the presence of an electric field, and finally the details of the derivation of the spin current are presented.

In the process of re-deriving all the equations in this paper, we have found a slightly different approach to solving the coupled set of differential equations Eq. 2.10 and explaining some of the details.

## 2.2 Rashba Hamiltonian

Rashba Hamiltonian can be accurately derived from Dirac equation by expanding it in powers of  $v/c$ . The second-order correction is providing us with the spin-orbit coupling term of form

$$H_{SO} = -\frac{\lambda}{\hbar} \boldsymbol{\sigma} \cdot (\hat{\mathbf{z}} \times \mathbf{p}) \quad (2.1)$$

In order to understand the physical origin of this Hamiltonian we derive it from intuitive arguments. Given a coordinate system  $S$  in which there is an electric field  $\mathbf{E}$  and no magnetic field, let us make a Lorentz transformation to a system  $\bar{S}$  that is moving with constant velocity  $\mathbf{v}$  with respect to  $S$ .

$$\bar{\mathbf{E}} = \gamma \mathbf{E} \quad ; \quad \bar{\mathbf{B}} = -\frac{\gamma}{c^2} (\mathbf{v} \times \mathbf{E}), \quad (2.2)$$

where  $\gamma = (1 - v^2/c^2)^{-1/2}$  is the Lorentz factor. For  $v \ll c$ ,  $\gamma$  is approximately 1. Therefore, even if in the system  $S$  there is no magnetic field, upon Lorentz boost there is an effective magnetic field in the system  $\bar{S}$  which is perpendicular to both the velocity and the electric field.

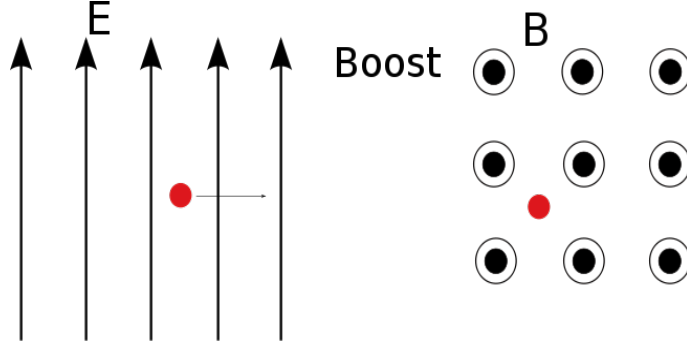


Figure 2.1: By performing a Lorentz boost from the laboratory frame to the frame which moves together with the electron, there is an effective magnetic field  $\mathbf{B}$  acting on the electron in the latter reference system.

Let us now consider an electron moving with velocity  $\mathbf{v}$  in an electric field in the  $\hat{\mathbf{z}}$  direction. Therefore in its own reference frame it experiences an effective magnetic field in the form of Eq. (2.2).

We can now find the spin-orbit Hamiltonian. Starting from the Hamiltonian of a magnetic moment interacting with a magnetic field

$$H = -\mu_{\mathbf{S}} \cdot \bar{\mathbf{B}}, \quad (2.3)$$

and taking into account that the electron's magnetic moment is proportional to the spin of the electron  $\mathbf{S} = \hbar\sigma/2$  we get

$$H_{SO} = -\frac{\lambda}{\hbar}\sigma \cdot (\hat{\mathbf{z}} \times \mathbf{p}). \quad (2.4)$$

We absorb all the coefficients in the spin-orbit coupling constant  $\lambda$ , including the magnitude of the electric field. From now on, we denote the effective magnetic field by  $\Delta = \frac{\lambda}{\hbar}(\hat{\mathbf{z}} \times \mathbf{p})$ .

## 2.3 A two-dimensional electron gas in a perpendicular electric field

We now consider a 2DEG in a perpendicular electric field  $\mathbf{E} = E\hat{\mathbf{z}}$ . The Hamiltonian for one electron is written as

$$H = \frac{p^2}{2m} - \frac{\lambda}{\hbar}\sigma \cdot (\hat{\mathbf{z}} \times \mathbf{p}). \quad (2.5)$$

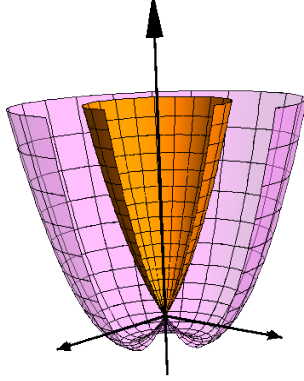


Figure 2.2: Cut through the plot of dispersion relations Eq.(2.6) [color online]. The outer band (purple) represents the  $E_-$  band, while the inner one (orange) is the  $E_+$  band.

The dispersion relation is a 3D body of rotation originating from a shifted parabola.

$$E_{\pm} = \frac{p^2}{2m} \pm \frac{\lambda}{\hbar} p \quad (2.6)$$

with the corresponding eigenspinors

$$\Psi_{\pm} = \frac{1}{\sqrt{2}} \begin{pmatrix} \pm i e^{-i\phi} \\ 1 \end{pmatrix},$$

with  $\phi$  the polar angle in the two-dimensional momentum space.

## 2.4 Landau-Lifshitz equation

Let us now apply to our 2DEG system another stationary electric field in the  $\hat{\mathbf{x}}$  direction,  $\mathbf{E} = E_x \hat{\mathbf{x}}$ . This induces a time-dependence of the momentum, and consequently of the effective magnetic field.

Let us obtain the dynamics of a spin 1/2 particle in a magnetic field. Equivalent to the spinor wavefunctions and Schrödinger equation for Hamiltonian (2.5) is the density matrix formalism. The density matrix in the general case is defined as

$$\rho = \sum_j p_j |\psi_j\rangle \langle \psi_j|, \quad (2.7)$$

where the coefficients  $p_j$  are non-negative and add up to one. For our particular case, the density operator is represented by a  $2 \times 2$  matrix. We can

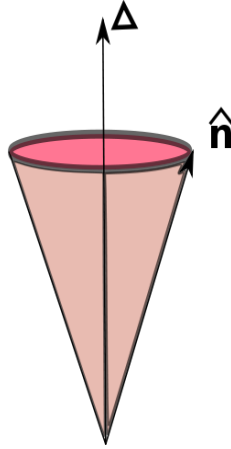


Figure 2.3: The equation (2.10) represents the spin precession about the magnetic field  $\Delta$ .

write the density matrix in the form

$$\rho = \frac{1}{2}(\mathbf{I}_2 + \mathbf{n} \cdot \sigma), \quad (2.8)$$

where  $\mathbf{I}_2$  is the  $2 \times 2$  unit matrix.

The factor  $1/2$  comes from the normalization condition  $Tr(\rho) = 1$ . Solving the Schrödinger equation for our Hamiltonian in the spinor basis is equivalent to solving

$$i\hbar \frac{d\rho}{dt} = [H, \rho] \quad (2.9)$$

in the density matrix formalism. From Eq. (2.8) it is straightforward to see that the time-derivative of the density matrix is easily expressed in terms of Pauli matrices  $\dot{\rho} = \frac{1}{2}\dot{\mathbf{n}} \cdot \sigma$ . Now the advantage of using the density matrix formalism becomes clear. Using Eq.(2.9) as well as the commutation relations of the Pauli matrices, one gets the Landau-Lifshitz equation:

$$\hbar \frac{d\hat{\mathbf{n}}}{dt} = \hat{\mathbf{n}} \times \Delta(t). \quad (2.10)$$

In this formalism the average value of the spin operator reads

$$Tr(\sigma\rho) = \langle \sigma \rangle = \mathbf{n}. \quad (2.11)$$

This shows the meaning of the vector  $\mathbf{n}$ : it represents the average spin projection in the density matrix formalism.

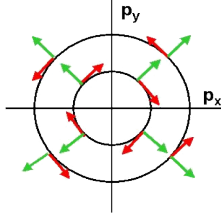


Figure 2.4: A cut through the dispersion relation Fig.(2.3) at the Fermi level. The green arrows represent the direction of momenta and the red ones are the orientation of the spins.

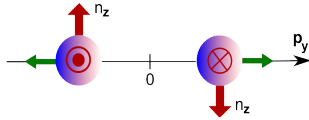


Figure 2.5: The spin displacement on the  $z$  component. The spin is perpendicular to the plane of the drawing. As in Fig.(2.4), the green arrows represent the momenta. The red arrows are the  $z$  components of the spins calculated in Eq.(2.13).

We therefore conclude that Eq.(2.10) describes the precession of the electron spin direction  $\hat{\mathbf{n}}$  around the magnetic field.

We project the Eq.(2.10) on some basis  $(\hat{\mathbf{x}}_1, \hat{\mathbf{x}}_2, \hat{\mathbf{x}}_3)$ , where at the initial moment the magnetic field  $\Delta$  points along  $\hat{\mathbf{x}}_1$ . The axis  $x_3$  is along the  $z$  direction. In order to solve the system of equations, we employ the following approximations. In the adiabatic limit, the spin rotates much faster than the momentum varies (and hence, the effective magnetic field). We are solving equations for spins in the linear response limit. From this follows that  $n_1(t)/n_2(t) = \Delta_1(t)/\Delta_2(t)$ , where  $\Delta_1 = \Delta(t) \cdot \hat{\mathbf{x}}_1$  and  $\Delta_2 = \Delta(t) \cdot \hat{\mathbf{x}}_2$  are the projections of the magnetic field on the axes. The meaning of this last relation is that the average spin direction  $\hat{\mathbf{n}}$  follows the magnetic field as it changes in time in the plane  $(\hat{x}_1, \hat{x}_2)$ .

Using these considerations, the solutions for the differential system of equations read

$$n_3 = \frac{\hbar}{\Delta_1^3} (\Delta \times \dot{\Delta})_3; \quad n_2 = \frac{\Delta_2}{\Delta_1}. \quad (2.12)$$

We identify the  $(\hat{\mathbf{x}}_1, \hat{\mathbf{x}}_2, \hat{\mathbf{x}}_3)$  system with an instant coordinate system in the momentum space such that  $\hat{\mathbf{x}}_3 \parallel \hat{\mathbf{z}}$  and  $\hat{\mathbf{x}}_2 \parallel \mathbf{p}$ . Since our approximations

imply that  $\Delta_1 \simeq \Delta$ , the  $\hat{\mathbf{z}}$ th component of the spin direction is

$$n_z = -\frac{\hbar^2}{2\lambda} e E_x \frac{p_y}{p^3}. \quad (2.13)$$

Due to the varying magnetic field, the spin is acquiring an out-of-plane component in the form of Eq.(2.13), which has a sign dependent on the  $y$  component of the momentum (see Fig. (2.4)).

## 2.5 Calculation of the spin current and spin resistivity

The  $i, j$  components of the spin current tensor is defined as

$$j_i^j = \frac{1}{2} \{S_i, v_j\} = \frac{\hbar}{4} \{\sigma_i, v_j\}. \quad (2.14)$$

It is straightforward to read the meaning: the current in the  $i, j$  direction is the anticommutator of the  $i$ th component of the spin with the  $j$ th component of the velocity. Its structure is similar to that of the charge current  $\mathbf{j} = q\mathbf{v}$  (with  $q = ne$  the charge density). The expression has to be antisymmetrized because the velocity depends on the spin.

A remarkable feature of the spin current Eq.(2.14) is the time reversal symmetry. Since both the spin and the velocity change sign upon time reversal, the spin current remains time-even. On the other hand, the charge current, which is proportional to the total charge and the velocity, changes sign upon time-reversal. The Ohm's law,

$$\mathbf{j} = \sigma \mathbf{E} \quad (2.15)$$

holds for both charge and spin current. The electric field is time-even. Then, the charge conductivity has to be time-odd, which means that it has to be proportional to a relaxation time  $\tau$ . But the spin-conductivity is time even, since both sides of Eq.(2.15) for spin currents are time-even. We can conclude that the spin-resistivity is allowed to be dissipationless. By calculating the spin current we will prove that this is indeed the case.

We are interested in calculating the spin current in the  $j = y, i = z$  direction. The  $v_y$  component of the velocity is calculated from Hamilton's equation

$$v_y = \frac{\partial H}{\partial p_y} = \frac{p_y}{m} + \frac{\lambda}{\hbar} \sigma_x. \quad (2.16)$$

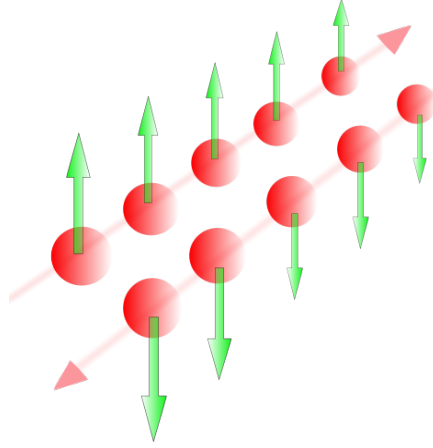


Figure 2.6: The spin current pictured as two counter-propagating spin-polarized charge currents.

Thus the current density is obtained

$$j_z^y = \frac{\hbar}{2m} \sigma_z p_y. \quad (2.17)$$

Using the  $z$ -th component of the average spin direction obtained in the previous section (Eq. (2.13)), we get the spin current density to be

$$j_z^y = -\frac{\hbar^3}{2m\lambda} e E_x \frac{p_y^2}{p^3}. \quad (2.18)$$

To get the total current we have to integrate over the whole Fermi sea. The integral is to be performed in momentum space. Let us consider both energy bands to be filled up, thus the Fermi level lies above the band-crossing point.

$$J_z^y = \int \frac{d\mathbf{p}}{(2\pi\hbar)^2} j_z^y f(E - E_F), \quad (2.19)$$

where  $f(E - E_F)$  is the Fermi-Dirac distribution function. We substitute the momentum components and element of volume in the  $\mathbf{p}$ -space as

$$\mathbf{p} = (p \cos \phi, p \sin \phi) \quad , \quad d\mathbf{p} = p dp d\phi \quad (2.20)$$

where  $\phi = (\mathbf{p}, \hat{\mathbf{x}})$  is the angle of the momentum vector with the  $x$ -axis. Since we are at  $T = 0K$ , the Fermi-Dirac distribution function becomes a

step function, so that the upper limit of the integration over  $p$  is the Fermi momentum  $p_F$ . With these considerations the current becomes

$$J_z^y = - \int_0^{2\pi} d\phi \int_0^{p_F} \frac{dp}{(2\pi\hbar)^2} \frac{\hbar^3}{2m\lambda} e E_x \sin^2 \phi. \quad (2.21)$$

Integration over the angle  $\phi$  is trivial and gives a factor of  $\pi$ . We will be left with a integral over all the momentum values, from 0 up to the Fermi momentum corresponding to the  $E_-$  band. But in the region between 0 and  $p_F^+$ , we have to sum contributions from both  $E_+$  and  $E_-$  band, which cancel each other because  $n_z$  for the two bands have equal magnitude and opposite sign. Therefore, the integral can be performed only over the annulus contained between the  $p_F^+$  and  $p_F^-$ , pictured in Fig.(2.4).

Thus the total current is

$$J_z^y = - \frac{\pi\hbar^3 e E_x}{4(2\pi\hbar)^2 m\lambda} (p_{F+} - p_{F-}). \quad (2.22)$$

The difference between the Fermi momenta for the two branches is obtained from the condition  $E_+(p_{F+}) = E_-(p_{F-})$  and equals  $-2m\lambda/\hbar$ . The final expression for the spin current reads

$$J_z^y = \frac{e}{8\pi} E_x. \quad (2.23)$$

Remarkably, the spin current depends only on the transverse electric field and has an universal resistivity of

$$\sigma_{yz}^S = \frac{e}{8\pi}, \quad (2.24)$$

dependent only on fundamental constants and independent of electron density or spin-orbit coupling.

## 2.6 Further remarks and conclusions

In calculating the spin current Eq.(2.23) we have made an assumption that both Rashba bands are filled. But if the Fermi level lies at or below the band-crossing point the spin-resistivity will not be universal anymore. That is because the contributions from the  $E_+$  and  $E_-$  bands on the momentum range  $(0, p_F^+)$  will not cancel anymore (there will be no contribution from the  $E_+$  band).



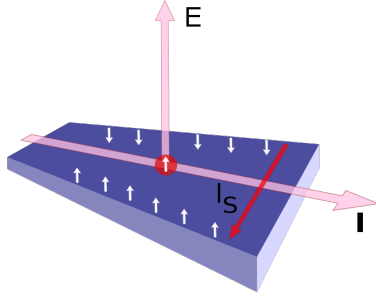


Figure 2.7: The spin current produced by the varying magnetic field produces a charge accumulation at the sample edges, similar to the Hall effect for charge currents.

In this chapter we have shown that in a two-dimensional electron gas with Rashba spin-orbit coupling, an electric field produces a spin-current which is perpendicular to the charge current. This is an intrinsic effect, similar to the intrinsic character of the anomalous Hall effect in some ferromagnets and strongly polarized paramagnets [12, 13]. The spin current Eq.(2.23) leads to spin accumulation at the sample edges. However, the spin relaxation limits the amount of spin accumulated at the boundaries.

In such systems, in a clean sample, where the transport scattering rate  $\tau^{-1}$  is small compared to the spin-orbit splitting  $\lambda k_F/\hbar$ , one finds an intrinsic value  $e/8\pi$  for the spin Hall conductivity, which is valid at finite frequencies in the range  $\tau^{-1} < \omega < \lambda k_F/\hbar$ , independent of details of the impurity scattering, in the usual case where both spin-orbit split bands are occupied. The prediction for the dc spin Hall effect in this model has been examined and debated extensively. It was first noticed that contributions to the spin-current from impurity scattering, even in the limit of weak disorder, seemed to cancel exactly the intrinsic contribution [14, 15]. This led to speculation that this cancellation destroys the effect in other models as well. Recent studies showed that such cancellation only occurs for this very particular model, due to the linearity of the spin-orbit coupling and the parabolic band dispersion [16, 17, 18, 19].

# Chapter 3

## Spin-Hall effect in hole-doped semiconductors

### 3.1 Introduction

The quantum Hall effect is a manifestation of quantum mechanics at a macroscopic scale. In contrast to usual transport coefficients in solid-state systems which are determined by scattering rates, the Hall conductance is quantized and completely independent of any scattering rates in the system. The transport equation is given by  $j_\alpha = \sigma_H \epsilon_{\alpha\beta} E_\beta$ , where  $\epsilon_{\alpha\beta}$  is the fully antisymmetric tensor in two dimensions. While the dissipative transport coefficients depend on the states near the Fermi level, the non-dissipative transport coefficients are expressed in terms of the equilibrium response of all the states below the Fermi level. Murakami et al. [1] have found a similar relation for a dissipationless spin current,

$$j_j^i = \sigma_S \epsilon^{ijk} E_k. \quad (3.1)$$

This fundamental response equation shows that it is possible to introduce a purely topological and dissipationless spin current by an electric field. The zero-frequency spin resistivity included in Eq. (3.1) does not depend on time since both parts of the equation are time-even. By this consideration, the resistivity can be independent of time, hence, dissipationless. On the other hand, in the Ohm's law the charge current is time-odd, while the electric field is time-even, which is why the conductivity must be inversely proportional to the relaxation time. From the above analysis, we see that there is a fundamental difference between the ordinary irreversible electronics based on Ohm's law and reversible spintronics computation based on Eq.(3.1).

In the next section we consider a realization of this electric field-induced spin current in conventional hole-doped semiconductors.

## 3.2 $\mathbf{k} \cdot \mathbf{p}$ approximation and Luttinger model

The  $\mathbf{k} \cdot \mathbf{p}$  approximation is the standard model for semiconductors. The Luttinger model is based on the  $\mathbf{k} \cdot \mathbf{p}$  method, where using symmetry considerations one determines the allowed terms in the Hamiltonian. We will briefly summarize the basic aspects of the Luttinger Hamiltonian for semiconductors. For a more comprehensive discussion of the model see Appendix A.

In isolated atoms spin-orbit coupling leads to a splitting the p-orbitals into four-fold degenerate  $P_{3/2}$  and two-fold degenerate  $P_{1/2}$  levels. In most semiconductors like Si, Ge and GaAs, the  $P_{3/2}$  form the top of valence bands, which are separated by the band gap from  $S$ -like conduction bands. Therefore, at the  $\Gamma$  point the valence bands are four-fold degenerate and the conduction bands are two-fold degenerate (see Fig. (3.2)). The form of the effective Hamiltonian can be determined from symmetry considerations alone. In crystals with inversion symmetry band energies depend quadratically on the momentum away from the  $\Gamma$  point. Therefore, a rotationally invariant Hamiltonian can only contain two possible terms:  $\mathbf{k}^2$  and  $(\mathbf{k} \cdot \mathbf{S})^2$ , where  $\mathbf{S}$  is the  $2 \times 2$  Pauli matrix for the two-fold conduction band and respectively the  $4 \times 4$  spin matrix for the four-fold valence band. To the lowest order, there is no spin-orbit coupling in the conduction band, as each Pauli matrix squared is the unity matrix. As the square of the spin 3/2 matrices is non-trivial, these two terms combine to form an effective Luttinger Hamiltonian for holes [20]:

$$H_0 = \frac{\hbar^2}{2m} \left[ \left( \gamma_1 + \frac{5}{2} \gamma_2 \right) k^2 - 2\gamma_2 (\mathbf{k} \cdot \mathbf{S})^2 \right] \quad (3.2)$$

This is equivalent to the more common used form

$$H_0 = \frac{\hbar^2}{2m} \left[ \left( \gamma_1 + \frac{5}{2} \gamma_2 \right) k^2 - 2\gamma_2 (k_x^2 S_x^2 + k_y^2 S_y^2 + k_z^2 S_z^2) - 4\gamma_3 \left( k_x k_y \{S_x, S_y\} + k_x k_z \{S_x, S_z\} + k_y k_z \{S_y, S_z\} \right) \right],$$

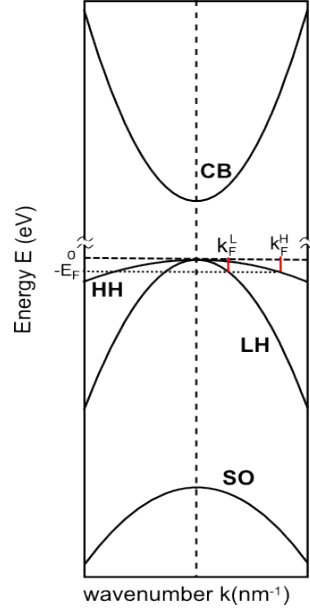


Figure 3.1: Approximative band structure of GaAs.

where  $\gamma_3 = 2\gamma_2$ . The  $S_i$  are the spin 3/2 matrices with the expressions

$$S_x = \begin{pmatrix} 0 & \frac{\sqrt{3}}{2} & 0 & 0 \\ \frac{\sqrt{3}}{2} & 0 & 1 & 0 \\ 0 & 1 & 0 & \frac{\sqrt{3}}{2} \\ 0 & 0 & \frac{\sqrt{3}}{2} & 0 \end{pmatrix},$$

$$S_y = \begin{pmatrix} 0 & -\frac{\sqrt{3}}{2}i & 0 & 0 \\ \frac{\sqrt{3}}{2}i & 0 & -i & 0 \\ 0 & i & 0 & -\frac{\sqrt{3}}{2}i \\ 0 & 0 & \frac{\sqrt{3}}{2}i & 0 \end{pmatrix}, \quad (3.3)$$

$$S_z = \begin{pmatrix} \frac{3}{2} & 0 & 0 & 0 \\ 0 & \frac{1}{2} & 0 & 0 \\ 0 & 0 & -\frac{1}{2} & 0 \\ 0 & 0 & 0 & -\frac{3}{2} \end{pmatrix}.$$

Good quantum numbers for this Hamiltonian are the helicity  $\lambda = \hbar^{-1}\mathbf{k} \cdot \mathbf{S}/k$  and the total angular momentum  $\mathbf{J} = \mathbf{l} + \mathbf{S} = \hbar\mathbf{x} \times \mathbf{k} + \mathbf{S}$ .

This kinetic Hamiltonian is diagonalized in the basis where the helicity operator  $\lambda$  is diagonal and the eigenvalue is given by

$$\epsilon_\lambda(\mathbf{k}) = \frac{\hbar^2 k^2}{2m} \left( \gamma_1 + \left( \frac{5}{2} - 2\lambda^2 \right) \gamma_2 \right) \equiv \frac{\hbar^2 k^2}{2m_\lambda} \quad (3.4)$$

This can formally be obtained by substituting the operator  $\mathbf{k} \cdot \mathbf{S}$  by  $\hbar k \lambda$  using the definition of helicity.

For a given wavevector the Hamiltonian (Eq. 3.2) has two eigenvalues,

$$\epsilon_H(\mathbf{k}) = \epsilon_{\lambda=\pm 3/2}(\mathbf{k}) = \frac{\gamma_1 - 2\gamma_2}{2m} \hbar^2 k^2 \equiv \frac{\hbar^2 k^2}{2m_H} \quad (3.5)$$

and

$$\epsilon_L(\mathbf{k}) = \epsilon_{\lambda=\pm 1/2}(\mathbf{k}) = \frac{\gamma_1 + 2\gamma_2}{2m} \hbar^2 k^2 \equiv \frac{\hbar^2 k^2}{2m_L}. \quad (3.6)$$

Equations (3.5) and (3.6) define the effective mass for the heavy and light holes respectively:  $m_H = m/(\gamma_1 - 2\gamma_2)$  and  $m_L = m/(\gamma_1 + 2\gamma_2)$ .

### 3.3 Introducing an electric field in the Luttinger Hamiltonian

Let us consider the effect of a uniform electric field  $\mathbf{E}$ . The full Hamiltonian is

$$H = H_0 + V(\mathbf{x}), \quad (3.7)$$

where  $V(\mathbf{x}) = e\mathbf{E} \cdot \mathbf{x}$  with  $-e$  the electron's charge and  $H_0$  given by Eq. (3.2).

We make an unitary transformation  $U(\mathbf{k})$  which is  $\mathbf{k}$ -dependent and orients locally the  $\mathbf{z}$  axis along  $\mathbf{k}$ , by rotation with  $\theta$  around  $S_y$  and respectively rotation by  $\phi$  around  $S_z$ . The expression for the unitary transformation is  $U = e^{i\theta S_y} e^{i\phi S_z}$ . Under this transformation the new Hamiltonian

$$\tilde{H} \equiv U(\mathbf{k}) H U^\dagger(\mathbf{k}) \quad (3.8)$$

becomes

$$\tilde{H} = \frac{\hbar^2 k^2}{2m} \left( \gamma_1 + \frac{5}{2} \gamma_2 - 2\gamma_2 S_z^2 \right) + U(\mathbf{k}) V(\mathbf{x}) U^\dagger(\mathbf{k}). \quad (3.9)$$

Let's check that the matrix elements of the Hamiltonian stay the same. Using the definition of the transformed fields we get

$$\langle \tilde{\Psi} | \tilde{H} | \tilde{\Psi} \rangle = \overbrace{\langle \tilde{\Psi} |} U^\dagger \overbrace{U H U^\dagger}^{\tilde{H}} \overbrace{| \tilde{\Psi} \rangle} U = \langle \Psi | H | \Psi \rangle,$$

where we used unitarity of the rotation matrix  $U^\dagger U = 1$ .

In the momentum space  $x$  becomes  $i\partial/\partial k \equiv i\partial_k$ , because they do not commute. Therefore the electric potential in momentum space includes the derivative with respect to momentum, as follows

$$V(\mathbf{x}) = e\mathbf{E} \cdot \mathbf{x} = e\mathbf{E} i \frac{\partial}{\partial \mathbf{k}}.$$

Upon the unitary transformation  $U(\mathbf{k})$  the potential term is rewritten as

$$U(\mathbf{k})V(\mathbf{x})U^\dagger(\mathbf{k}) = U(\mathbf{k})\left(e\mathbf{E} \cdot \mathbf{x}\right)U^\dagger(\mathbf{k}) = e\mathbf{E}\left(U(\mathbf{k})i\frac{\partial}{\partial \mathbf{k}}U^\dagger(\mathbf{k})\right).$$

This is still an operator, so the expansion follows

$$e\mathbf{E}\left(i\frac{\partial}{\partial \mathbf{k}} + iU_k\frac{\partial U_k^\dagger}{\partial \mathbf{k}}\right).$$

We define the covariant derivative by  $\tilde{\mathbf{D}} = i\partial_k - \tilde{\mathbf{A}}$  and  $\tilde{\mathbf{A}} = -iU(\mathbf{k})\partial_k U^\dagger(\mathbf{k})$ . The potential term has now the form

$$V(\tilde{\mathbf{D}}) = e\mathbf{E} \cdot \tilde{\mathbf{D}}.$$

The field  $\tilde{\mathbf{A}}$  is a pure gauge potential, so there is no curvature associated with it. This is not a pure gauge in sense of Maxwell electrodynamics, because the generators do not commute. In non-Abelian theory the gauge transformation is an operator in itself.

The unitary operator that expresses the gauge transformation is  $U = e^{i\theta S_y} e^{i\phi S_z}$ , as we have mentioned above. This is now a  $4 \times 4$  matrix, and it has three generators  $S_x, S_y$  and  $S_z$  which form a Lie algebra. Therefore, the vector potential is a linear superposition of the generators of the group.

In the Maxwell form (Abelian theory), the electromagnetic field strength tensor is

$$F_{\mu\nu} = \partial_\mu A_\nu - \partial_\nu A_\mu.$$

The  $0i$ -th component of the tensor and the component  $ij$  is proportional to the  $\varepsilon_{ijk}$  times magnetic field.

For non-Abelian theory  $F_{\mu\nu}$  is an operator (in our case a spin operator), and the definition of the strength field tensor is accordingly

$$F_{\mu\nu} = \tilde{D}_\mu \tilde{A}_\nu - \tilde{D}_\nu \tilde{A}_\mu.$$

The long derivatives  $D_\mu$  are of the form  $\partial_\mu - A_\mu^a S^a$ . In Abelian theories the generators are 1. For a non-Abelian theory, this is not the case anymore, so we decompose the vector potential over the generators of the Lie group:  $A_\mu = A_\mu^a S^a$ .

Recalling the expression for the long derivative  $\tilde{D} = i\partial_\mu - A_\mu$ , we have

$$F_{\mu\nu} = i(\partial_\mu A_\nu - \partial_\nu A_\mu) + A_\nu A_\mu - A_\mu A_\nu \equiv i(\partial_\mu A_\nu - \partial_\nu A_\mu) - [A_\mu, A_\nu] \quad (3.10)$$

In the Abelian theories the commutator  $[A_\mu, A_\nu]$  is zero.

In order to prove that  $F_{\mu\nu}$  is zero let us replace the definition  $A_\mu = -iU\partial_\mu U^\dagger$  in Eq. (3.10):

$$\begin{aligned} F_{\mu\nu} &= \left[ \partial_\mu (U\partial_\nu U^\dagger) - \partial_\nu (U\partial_\mu U^\dagger) \right] - \left[ -iU\partial_\mu U^\dagger, -iU\partial_\nu U^\dagger \right] \\ &= \left( \partial_\mu U\partial_\nu U^\dagger + U\partial_\mu\partial_\nu U^\dagger - \partial_\nu U\partial_\mu U^\dagger - U\partial_\nu\partial_\mu U^\dagger \right) \\ &\quad - \left( -U(\partial_\mu U^\dagger)U\partial_\nu U^\dagger + U(\partial_\nu U^\dagger)U\partial_\mu U^\dagger \right). \end{aligned}$$

The second and the third term are equal and of opposite sign and the terms coming from the commutator can be simplified using the unitarity of  $U$ . Using  $UU^\dagger = 1$  one gets the product of  $U$ -s as follows

$$(\partial_\mu U)U^\dagger + U\partial_\mu U^\dagger = 0 \quad \Rightarrow \quad (\partial_\mu U)U^\dagger = -U(\partial_\mu U^\dagger). \quad (3.11)$$

Henceforth, the field strength tensor acquires the expression

$$\begin{aligned} F_{\mu\nu} &= \left( \partial_\mu U\partial_\nu U^\dagger - \partial_\nu U\partial_\mu U^\dagger \right) + \left( -(\partial_\mu U)U^\dagger U\partial_\nu U^\dagger + (\partial_\nu U)U^\dagger U\partial_\mu U^\dagger \right) \\ &= \partial_\mu U\partial_\nu U^\dagger - \partial_\nu U\partial_\mu U^\dagger - \partial_\mu U\partial_\nu U^\dagger + \partial_\nu U\partial_\mu U^\dagger \\ &= 0. \end{aligned}$$

We have thus proven that the field  $A_\mu$  has no curvature associated with it and hence is a pure gauge potential for our non-Abelian theory.

Up to this point the transformation is exact. We now make an approximation by considering adiabatic transport. As usual done in transport theory, we neglect the interband transitions, i.e., the off-block-diagonal elements of  $\tilde{\mathbf{A}}$  connecting the light-hole and heavy-hole bands. For  $U(k) = e^{i\theta S_y} e^{i\phi S_z}$ , the gauge field  $\tilde{\mathbf{A}}$  is

$$\begin{aligned}\tilde{\mathbf{A}} &= -iU\partial_{\mathbf{k}}U^\dagger \\ &= -ie^{i\theta S_y} e^{i\phi S_z} \left[ -i(\partial_{\mathbf{k}}\phi)S_z e^{-i\phi S_z} e^{-i\theta S_y} - ie^{-i\phi S_z} S_y (\partial_{\mathbf{k}}\theta) e^{-i\theta S_y} \right] \\ &= (-S_z \cos \theta + S_x \sin \theta) \partial_{\mathbf{k}}\phi - S_y \partial_{\mathbf{k}}\theta,\end{aligned}$$

where in the last step we've used the commutation relations of the spin matrices  $[S_y, S_z] = iS_x$ . By employing the explicit form of the spin matrices (see Eq. (3.3)), the gauge connection is written explicitly as

$$\tilde{\mathbf{A}} \cdot d\mathbf{k} = \begin{pmatrix} -\frac{3}{2} \cos \theta d\phi & \frac{\sqrt{3}}{2} (\sin \theta d\phi + id\theta) & 0 & 0 \\ \frac{\sqrt{3}}{2} (\sin \theta d\phi - id\theta) & -\frac{1}{2} \cos \theta d\phi & \sin \theta d\phi + id\theta & 0 \\ 0 & \sin \theta d\phi - id\theta & -\frac{1}{2} \cos \theta d\phi & \frac{\sqrt{3}}{2} (\sin \theta d\phi + id\theta) \\ 0 & 0 & \frac{\sqrt{3}}{2} (\sin \theta d\phi - id\theta) & \frac{3}{2} \cos \theta d\phi \end{pmatrix},$$

where the first and fourth columns correspond to the heavy-hole (HH) band, while the second and the third ones correspond to the light-hole (LH) band. In considering adiabatic transport, we neglect the interband transitions, i.e. the off-block-diagonal matrix elements of  $\tilde{\mathbf{A}}$  between the LH and HH bands. We then arrive at a non-trivial adiabatic gauge connection

$$\mathbf{A}' \cdot d\mathbf{k} = \begin{pmatrix} -\frac{3}{2} \cos \theta d\phi & 0 & 0 & 0 \\ 0 & -\frac{1}{2} \cos \theta d\phi & \sin \theta d\phi + id\theta & 0 \\ 0 & \sin \theta d\phi - id\theta & -\frac{1}{2} \cos \theta d\phi & 0 \\ 0 & 0 & 0 & \frac{3}{2} \cos \theta d\phi \end{pmatrix}, \quad (3.12)$$

which takes a block-diagonal form in the LH and HH subspace. As the states in each subspace are two-fold degenerate, the gauge connection is in general non-Abelian. However, the non-Abelian structure is only present in the LH band. Namely, in the LH subspace the matrix  $\mathbf{A}'$  has off-diagonal components, while in the HH subspace  $\mathbf{A}'$  is diagonal. This is because the gauge field  $\tilde{\mathbf{A}}$  connects states with helicity difference  $\Delta\lambda = 0, \pm 1$ , and does not connect  $\lambda = \pm 3/2$  states in the HH band.

In the next section we take a step back and consider the Abelian approximation. Later on, we will compute the physical quantities also in the full non-Abelian treatment.



### 3.4 Abelian approximation

For simplicity of presentation, we shall first make the Abelian approximation. By employing this approximation, we neglect the non-diagonal elements of  $\mathbf{A}'$  and Eq. (3.12) becomes

$$\mathbf{A}'_{Abelian} = -S_z \cos \theta \nabla \phi, \quad (3.13)$$

which is diagonal in the basis where  $S_z$  is diagonal. As has been recognized in [21] the band-touching point acts as the source of the monopole field in momentum space. Thus each diagonal component of  $\mathbf{A}'$  is given by that of a Dirac monopole at  $\mathbf{k} = 0$  with the monopole strength  $eg$  given by  $S_z$ , in accordance with [21]. The associated magnetic field strength is given by

$$F_{ij} \equiv i[D_i, D_j] = \epsilon_{ijl} \lambda \frac{k_l}{k^3}. \quad (3.14)$$

An effective Hamiltonian has the form

$$H^{eff} = \frac{\hbar^2 k^2}{2m_\lambda} + V(\mathbf{x}). \quad (3.15)$$

Henceforth,  $x_i$  denotes the covariant derivative in momentum space:  $x_i \equiv D_i \equiv i\partial/\partial k_i - A_i(\mathbf{k})$ . The definition of  $x_i$  has changed by projecting the original Hamiltonian  $H$  onto the HH or LH band. Whereas  $H^{eff}$  seems to be trivial, its non-trivial dynamics are revealed through the nontrivial commutation relations

$$[k_i, k_j] = 0 \quad , \quad [x_i, k_j] = i\delta_{ij} \quad , \quad [x_i, x_j] = -F_{ij}. \quad (3.16)$$

These relations resemble the nontrivial commutation relations between the position operators of a two-dimensional electron gas projected onto the lowest Landau level.[22], where  $F_{ij} = B\epsilon_{ij}$ , and  $B$  is the external magnetic field. This algebraic structure, called “non-commutative geometry” arises in this case from the magnetic monopole in momentum space, and is a natural generalization of the quantum-Hall effect in three dimensions.

Equations of motion can easily be derived by replacing the Hamiltonian (3.15) in Heisenberg equations:  $i\hbar\dot{\mathbf{k}} = [\mathbf{k}, H]$ ,  $i\hbar\dot{\mathbf{x}} = [\mathbf{x}, H]$  and by using the commutation relations (3.16). Equations of motion for holes thus read

$$\hbar\dot{k}_i = eE_i, \quad \dot{x}_i = \frac{\hbar k_i}{m_\lambda} + F_{ij}\dot{k}_j \quad (3.17)$$

The last term, proportional to  $F_{ij}$ , is a topological term, describing the effect of the magnetic monopole on the orbital motion. It represents a ‘‘Lorentz force’’ in momentum space, making the hole velocity noncollinear with its momentum. In fact, if we interchange the roles of  $x$  and  $k$  in this equation, this term becomes the Lorentz force for a charged particle, moving in the presence of a magnetic monopole in real space.

In the Abelian approximation the set of coupled equations (3.17) can be integrated analytically. The first equation is straightforwardly integrated to give

$$k_i(t) = k_i(0) + \frac{eE_i}{\hbar}t. \quad (3.18)$$

The details of integrating the second equation are given in Appendix B. When  $\mathbf{E}$  is parallel to  $+z$  direction, the solutions are

$$k_x(t) = k_{x0}, \quad k_y(t) = k_{y0}, \quad k_z(t) = k_{z0} + eE_z t/\hbar, \quad (3.19)$$

$$z(t) = z_0 + \frac{\hbar k_{z0}}{m_\lambda} + \frac{eE_z}{2m_\lambda}t^2, \quad (3.20)$$

$$x(t) = x_0 + \frac{\hbar k_{x0}}{m_\lambda}t - \frac{\lambda k_{y0}}{k_{x0}^2 + k_{y0}^2} \frac{eE_z t/\hbar + k_{z0}}{\sqrt{k_{x0}^2 + k_{y0}^2 + (eE_z t/\hbar + k_{z0})^2}} \quad (3.21)$$

$$y(t) = y_0 + \frac{\hbar k_{y0}}{m_\lambda}t + \frac{\lambda k_{x0}}{k_{x0}^2 + k_{y0}^2} \frac{eE_z t/\hbar + k_{z0}}{\sqrt{k_{x0}^2 + k_{y0}^2 + (eE_z t/\hbar + k_{z0})^2}}. \quad (3.22)$$

The last terms in  $x(t)$  and  $y(t)$  represent a shift of the particle position, in a direction perpendicular to  $\mathbf{k}$ , as presented in Fig.(3.4). As the direction of the spin is parallel(antiparallel) to  $\mathbf{k}$  for  $\lambda > 0$  ( $\lambda < 0$ ), the hole motion in real space obtains a shift perpendicular to  $\mathbf{S}$ . This shift is analogous to the deflection of a charged article by a magnetic field monopole in a direction perpendicular to the plane spanned by its position and velocity vectors [23]. It causes a spin current perpendicular to both  $\mathbf{E}$  and  $\mathbf{S}$ , which we will briefly discuss in the next paragraph.

The motion along the  $z$ -direction in the equation (3.17) is free acceleration by the electric field. In reality, because this acceleration is suppressed by random scattering we should take into account the charge relaxation by random scattering.

The spin current in the  $y$ -direction with spin parallel to the  $x$ -axis for each

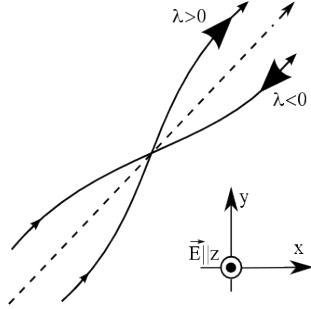


Figure 3.2: Real space trajectory of the hole obtained by solving Eq. (3.17).

band at zero temperature is given by

$$j_y^{xH} = \frac{\hbar}{3} \sum_{\lambda=\pm\frac{3}{2}, \mathbf{k}} \dot{y} \frac{\lambda k_x}{k} n^\lambda(\mathbf{k}) = \frac{3e}{2} E_z \sum_{\mathbf{k}} \frac{n^H(\mathbf{k}) k_x^2}{k^4} = \frac{e E_z k_F^H}{4\pi^2}, \quad (3.23)$$

$$j_y^{xL} = \frac{\hbar}{3} \sum_{\lambda=\pm\frac{1}{2}, \mathbf{k}} \dot{y} \frac{\lambda k_x}{k} n^\lambda(\mathbf{k}) = \frac{e}{6} E_z \sum_{\mathbf{k}} \frac{n^L(\mathbf{k}) k_x^2}{k^4} = \frac{e E_z k_F^L}{36\pi^2}, \quad (3.24)$$

where  $n^\lambda(\mathbf{k})$  is a filling of holes in the band with helicity  $\lambda$ ,  $n^{\pm 3/2}(\mathbf{k}) = n^H(\mathbf{k})$  and  $\lambda$ ,  $n^{\pm 1/2}(\mathbf{k}) = n^L(\mathbf{k})$  are fillings for the HH and LH bands, respectively. Charge relaxation is already included in this result by putting the Fermi surface as in their equilibrium position  $|\mathbf{k}| = k_F$ . We have taken into account that the expectation value of the electron spin is  $\mathbf{s} = \frac{1}{3}\mathbf{S}$ . This is because the spin-3/2 matrix  $\mathbf{S}$  is a sum of the spin angular momentum  $\mathbf{s}$  with spin one-half and the atomic orbital angular momentum  $\mathbf{l}$  with spin one [20]. By summing up the contributions to the spin currents from the two bands, namely Eq. (3.23) and Eq.(3.24), the spin current at zero temperature, with spin parallel to the  $x$  axis, flowing to the  $y$  direction reads

$$j_y^x = \frac{e E_z}{36\pi^2} (9k_F^H + k_F^L). \quad (3.25)$$

We have thus obtained an expression for the spin current which has the same form as Eq.(3.1). The spin resistivity is dissipationless and for a given band-structure is completely determined by the Fermi momenta corresponding to the HH and LH bands.

Here we have assumed that equilibrium momentum distribution is attained by random impurity scattering that causes the charge relaxation. These extrinsic effects are small [1]. The formula Eq.(3.25) is valid for zero temperature; for finite temperature, it is modified only thorough the Fermi distribution function  $n^\lambda(\mathbf{k})$ . For example, at room temperature and  $n = 10^{19}\text{cm}^{-3}$ ,

the nominal value of the energy difference between the LH and HH bands at the same wavenumber is 0.1eV, and it is much larger than both the temperature ( $\sim 0.025\text{eV}$ ) and the energy scale for momentum relaxation  $\hbar/\tau_p \sim 0.006\text{eV}$ , where we estimated the momentum relaxation time  $\tau_p$  to be of the same order as the spin relaxation for holes  $\tau_s \sim 100\text{fsec}$ . Thus the value of the spin current remains of the same order of magnitude as in the zero temperature case. Furthermore, these small effects scale with a higher power of  $k_F \sim n^{1/3}$  and extrapolating to the limit of  $n \rightarrow 0$ , the constant intercept would uniquely determine the predicted dissipationless spin conductivity.

It is worth noting that this Abelian approximation becomes exact in zero-gap semiconductors, e.g.,  $\alpha\text{-Sn}$ . In this class of materials the bottom of the conduction band and the top of the valence band correspond to the LH and HH bands in other semiconductors such as GaAs. These two bands touch at  $\mathbf{k} = 0$ . In this case, p-doping introduces holes only in the HH band, and the Abelian approximation becomes exact. This is of great importance for the quantum spin-Hall effect (which is analogous to the effect discussed in this thesis, but where the spin conductivity is quantized). It has been predicted to arise in zero-gap semiconductor heterojunctions [24].

### 3.5 Non-Abelian spin current

We now discuss the correction due to the non-Abelian nature of the gauge connection of the LH band. Remarkably, even though the gauge connection is non-Abelian, the associated field strength is Abelian, and is given by [25]

$$F_{ij} = \epsilon_{ijl} \lambda \left( 2\lambda^2 - \frac{7}{2} \right) \frac{k_l}{k^3}. \quad (3.26)$$

As the spin current depends only on the field strength in momentum space, the spin current acquires an extra factor of (-3) only for the LH band, compared with the Abelian approximation. Equations of motion for the non-Abelian theory can be solved numerically. Using Eq.(3.26) we obtain the following expression for the spin current:

$$\begin{aligned} j_y^x &= \frac{\hbar}{3} \text{tr} \sum_{\mathbf{k}} \dot{y}^n(\mathbf{k}) S_x n^\lambda(\mathbf{k}) = \frac{eE_z}{3} \text{tr} \sum_{\mathbf{k}} F_{yz}(\mathbf{k}) S_x n^\lambda(\mathbf{k}) \\ &= \frac{eE_z}{3} \text{tr} \sum_{\mathbf{k}} \frac{k_x S_x}{k^3} \lambda \left( 2\lambda^2 - \frac{7}{2} \right) n^\lambda(\mathbf{k}) = \frac{eE_z}{9} \text{tr} \sum_{\mathbf{k}, \lambda} \frac{1}{k^2} \lambda^2 \left( 2\lambda^2 - \frac{7}{2} \right) n^\lambda(\mathbf{k}) \\ &= \frac{eE_z}{12\pi^2} (3k_F^H - k_F^L). \end{aligned}$$

The same discussion about the temperature and scattering dependence holds here as well. By defining the spin conductivity to have the same dimension as the electrical conductivity, this last result can be written as

$$j_y^x = \frac{eE_z}{12\pi^2}(3k_F^H - k_F^L) = \frac{\hbar}{2e}\sigma_s E_z. \quad (3.27)$$

The  $xy$  component of the spin current tensor is rotationally invariant, with the covariant form given in (3.1). It results in a spin accumulation at the edges of the sample. This accumulation is limited by the spin relaxation. In the bulk, our spin current is free from rapid relaxations of the spin holes, because it is a purely quantum mechanical effect with equilibrium spin-momentum distribution. Nevertheless, at the sample boundaries the spin-momentum distribution deviates from equilibrium and the rapid relaxation of hole spins becomes effective.

### 3.6 Spin current obtained from conservation of the total angular momentum

The spin current introduced by the electric field can also be understood in terms of the conservation of the total angular momentum  $\mathbf{J} = \hbar\mathbf{x} \times \mathbf{k} + \mathbf{S}$ . As remarked earlier,  $\mathbf{J}$  commutes with  $H_0$ . When  $\mathbf{E}$  is parallel to the  $z$  direction,  $J_z$  also commutes with the potential. Therefore, substituting  $\mathbf{S} = \lambda\hbar\hat{\mathbf{k}} = \lambda\hbar\mathbf{k}/k$ , we obtain

$$\dot{J}_z = \hbar(\dot{\mathbf{x}} \times \mathbf{k})_z + \hbar(\mathbf{x} \times \dot{\mathbf{k}})_z + \lambda\hbar\dot{\hat{\mathbf{k}}}_z = 0. \quad (3.28)$$

The second term, representing the torque, vanishes in our case because  $\dot{\mathbf{k}}$  points along the  $z$  direction. The first term  $\hbar(\dot{\mathbf{x}} \times \mathbf{k})_z$  vanishes in usual problems; however, not in our case, due to non-collinearity of the velocity and the momentum. Furthermore, the first term, describing the time derivative of the orbital angular momentum  $\mathbf{L} = \hbar\mathbf{x} \times \mathbf{k}$  is proportional to the spin current. The third term  $\lambda\hbar\dot{\hat{\mathbf{k}}}_z$ , describing the time derivative of the spin angular momentum  $\mathbf{S}$ , can easily be evaluated from the acceleration equation in Eq. (3.17). Therefore we see that the conservation of the total angular momentum in Eq. (3.28) directly implies the spin current in Eq.(3.25). The spin current flows in such a way that the change of  $\mathbf{L}$  exactly cancels the change of  $\mathbf{S}$ .

### 3.7 Further remarks and conclusions

In the Luttinger model for p-doped semiconductors such as Si, GaAs and Ge an external electric field induces a spin current.

In contrast to similar effects [7], this spin current has a topological character. The spin conductivity in Eq.(3.1) is independent of the mean free path and relaxation rates, and all states below the Fermi energy contribute to the spin current, where each contribution is determined purely by the gauge curvature in momentum space, similar to the quantum-Hall effect [26]. At finite temperature the equations for spin current Eq. (3.25),(3.27) are modified only through the Fermi distribution function  $n^\lambda(\mathbf{k})$ . Because the typical energy difference between the light hole(LH) and heavy hole(HH) bands at the same wavenumber is about 0.1 eV, which largely exceeds the energy scale of the room temperature  $\sim 0.025$  eV, this predicted effect remains of the same order of magnitude even at room temperature.

This spin current is also useful for spin injection into semiconductors. Usage of ferromagnetic metals is not practical because most of the spin polarizations are lost at the interface due to conductivity mismatch between the metal and semiconductor [27, 28]. The electric-field induced spin current serves as a spin injector, because it creates a spin current inside the semiconductor.

# Chapter 4

## Quantum spin Hall effect in semiconductor quantum wells

### 4.1 Introduction

In the search for topologically non-trivial states of matter, a new class of topological insulators has been proposed. These topological insulators have an insulating gap in the bulk, but have topologically protected edge states due to the time reversal symmetry. In two dimensions the helical edge states give rise to the quantum spin Hall (QSH) effect in the absence of any external magnetic field. In this chapter we review a recent theory which predicts that the QSH state can be realized in HgTe/CdTe semiconductor quantum wells. By varying the thickness of the quantum well, the band structure changes from a normal to an inverted type at a critical thickness  $d_c$ . We present an analytical solution for the helical edge states and explicitly demonstrate their topological stability. We also review the recent experimental observation of the QSH state in HgTe/(Hg,Cd)Te quantum wells.

Beyond the potential technological applications, the intrinsic spin Hall effect has guided the scientists in the search for new topologically non-trivial states of matter. The quantum Hall state gives the first, and so far the only example of a topologically non-trivial state of matter, where the quantization of the Hall conductance is protected by a topological invariant [26]. Given the fundamental importance of topological quantization in physics, it is highly desirable to search for quantum states of matter characterized by non-trivial topological properties similar to, but distinct from the quantum Hall state. Soon after the theoretical prediction of the intrinsic spin Hall

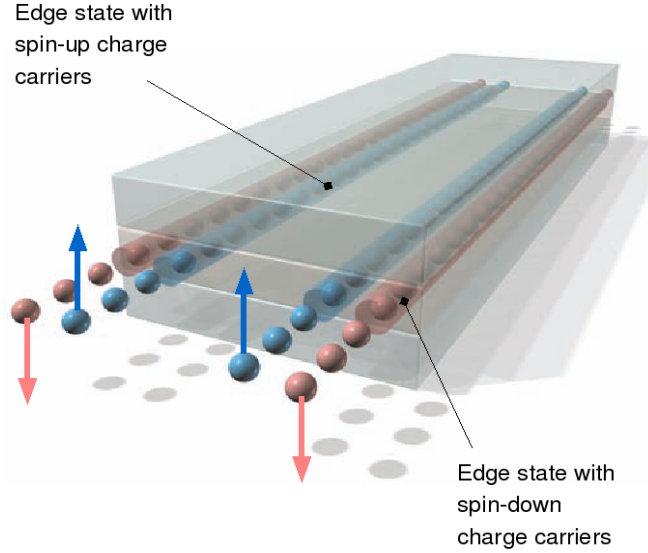


Figure 4.1: Schematic of the spin-polarized edge channels in a quantum spin Hall insulator. (from [3])

effect in doped semiconductors, a rather dramatic prediction was made that the intrinsic spin Hall effect could also be realized in insulators [29]. Subsequently, the QSH state was independently proposed in graphene [30] and in strained semiconductors [31]. The quantum spin-Hall insulator state is invariant under time reversal, has a charge excitation gap in the 2D bulk, but has topologically protected gapless edge states that lie inside the bulk insulating gap. The edge states have a distinct helical property: two states with opposite spin-polarization counter-propagate at a given edge [30, 32, 33] (see Fig. 4.1). For this reason they are also called helical edge states. The edge states come in Kramers doublets, and time reversal symmetry ensures the crossing of their energy levels at special points in the Brillouin zone. Because of this energy level crossing, the spectrum of a quantum spin-Hall insulator cannot be adiabatically deformed into that of a topologically trivial insulator without helical edge states; therefore, in this precise sense, the quantum spin-Hall insulators represent a topologically distinct new state of matter.

Recently the possibility of an intrinsic spin Hall effect has been put forward, which originates from the modification of the band structure of semiconductors due to spin-orbit coupling rather than from scattering from impurities [8]. Furthermore, the interest in the intrinsic spin-Hall effect has been enhanced by the possibility that such a spin current is quantized.



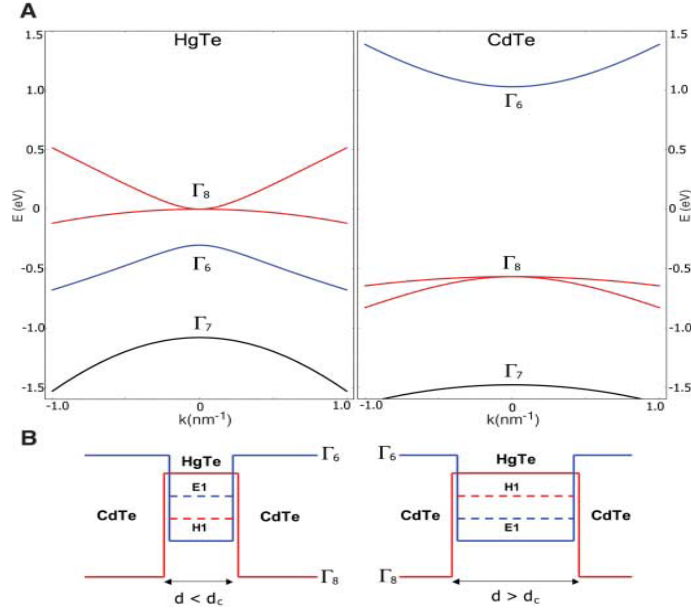


Figure 4.2: (A) Bulk energy bands of HgTe and CdTe near the  $\Gamma$  point. (B) The CdTe-HgTe-CdTe quantum well in the normal regime  $E1 > H1$  with  $d < d_c$  and in the inverted regime  $H1 > E1$  with  $d > d_c$ . In this and other figures,  $\Gamma_8/H1$  symmetry is indicated in red and  $\Gamma_6/E1$  symmetry is indicated in blue.(from [24])

## 4.2 Effective model for the quantum spin-Hall state in HgTe/CdTe quantum wells

The quantum spin-Hall is the cousin of quantum anomalous Hall effect, which is the charge Hall effect produced by internal magnetization rather than by external magnetic field. Consequently, extension of the model for the anomalous quantum Hall effect provided good grounds for the study of quantum spin-Hall effect [30, 34].

Inverted band-gap semiconductors are most likely realizations of a system showing the quantum spin-Hall effect and therefore a great deal of theoretical work has been focused on materials like graphene and HgTe. It turned out that graphene is not a good candidate, since the gap opened by spin-orbit coupling is too small. There is still a challenge to find more suitable materials in which quantum spin-Hall effect can be realized.

For zero-gap semiconductors, such as HgTe and CdTe, the important bands near the Fermi level are close to the  $\Gamma$  point in the Brillouin zone, and they

are s-type band (with  $\Gamma_6$  symmetry) and p-type band which is split into a  $J = 3/2$ -band ( $\Gamma_8$ ) and a  $J = 1/2$ -band by spin-orbit coupling. HgTe as a bulk material has a negative energy gap, which indicates that the  $\Gamma_8$  band, which usually forms the the valence band, is above the  $\Gamma_6$  band (see Fig. 4.2). The light-hole bulk subband of the  $\Gamma_8$  band becomes the conduction band, the heavy-hole bulk subband becomes the first valence band, and the s-type band ( $\Gamma_6$ ) is pushed below the Fermi level. Based on this unusual sequence of states, such a band structure is called inverted.

Quantum wells of the type III semiconductors provide a natural realization of the band-inversion [24]: the barrier material (e.g., CdTe) has a normal band progression, with the s-type band that has  $\Gamma_6$  symmetry lying above the p-type band that has  $\Gamma_8$  symmetry, and the well material (e.g., HgTe) having an inverted gap progression, as explained above. By tuning the quantum well thickness we can continuously pass from a normal band progression to a inverted band progression regime in the well material. In this “inverted” regime, which happens above a certain thickness  $d_c$ , it has been shown that the quantum spin-Hall state can be realized [24]. The level crossing which takes place at  $d_c$  is similar to the case of graphene, and furthermore, the electronic states near the  $\Gamma$  point are described by a relativistic Dirac equation in 2+1 dimensions.

In the models involving Luttinger-type of spin-orbit coupling there are topologically protected gapless bands of states localized at the edges of a semiconductor sample, as their energies lie in the gap of the bulk insulator. Once the spin-Hall effect is realized in the ground state, it is protected against thermal fluctuations by the bulk energy gap. These edge states have a distinct helical property: two states with opposite spin polarization counterpropagate at a given edge. [30, 24] (see picture 4.1). The origin of these chiral states is the Berry phase acquired by the holes moving in the momentum space, as we will briefly discuss in the next paragraph.

The starting point of the model is the two-band Luttinger effective Hamiltonian [20], in two spatial dimensions.

$$H_{eff}(k_x, k_y) = \begin{pmatrix} H(k) & 0 \\ 0 & H^*(-k) \end{pmatrix}, H = \varepsilon(k) + d_i(\mathbf{k})\sigma_i, \quad (4.1)$$

where  $\sigma_i$  are the Pauli matrices and  $d_i(\mathbf{k})$  are functions of the in-plane momenta and some material-specific constants. They represent the spin-orbit coupling as a function of momentum.

The Hamiltonian Eq.(4.1) can be easily diagonalized to obtain the two-band energy spectrum as  $E_{\pm}(\mathbf{k}) = \varepsilon(\mathbf{k}) \pm Vd(\mathbf{k})$ , in which  $d(\mathbf{k})$  is the norm of

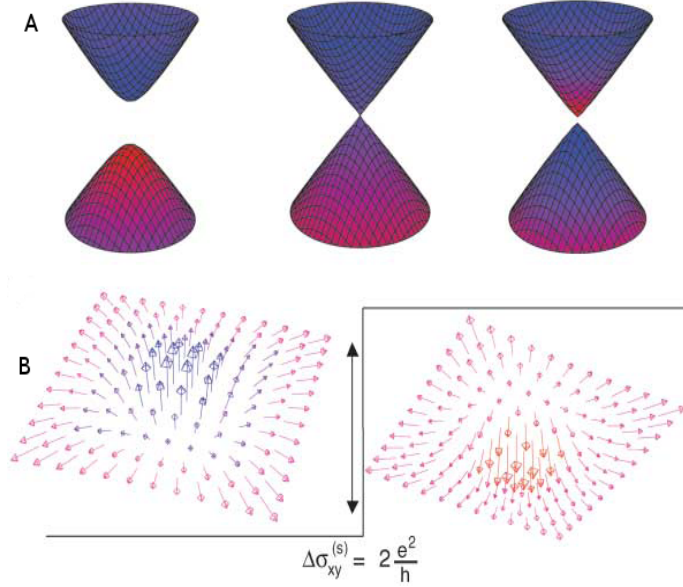


Figure 4.3: (A) Energy dispersion relations  $E(k_x, k_y)$  of the E1 and H1 subbands at  $d = 40, 63.5,$  and  $70$  (from left to right). Colored shading indicates the symmetry type of the band at that  $\mathbf{k}$  point. Places where the cones are more red indicate that the dominant state is H1 at that point; places where they are more blue indicate that the dominant state is E1. Purple shading is a region where the states are more evenly mixed. At  $40$ , the lower band is dominantly H1 and the upper band is dominantly E1. At  $63.5$ , the bands are evenly mixed near the band crossing and retain their  $d \uparrow$   $dc$  behavior moving farther out in  $\mathbf{k}$ -space. At  $70$ , the regions near  $k_{\parallel} = 0$  have flipped their character but eventually revert back to the  $d < dc$  farther out in  $\mathbf{k}$ -space. Only this dispersion shows the meron structure (red and blue in the same band). (B) Schematic meron configurations representing the  $\text{di}(\mathbf{k})$  vector near the  $\Gamma$  point. The shading of the merons has the same meaning as the dispersion relations above. The change in meron number across the transition is exactly equal to 1, leading to a quantum jump of the spin Hall conductance  $\sigma_{xy}^s = 2e^2/h$ . (from [3])

the three-vector  $d_\alpha(\mathbf{k})$ . The Hall conductivity can be calculated using the standard Kubo formula to be

$$\sigma_{xy} = \lim_{\omega \rightarrow 0} \frac{i}{\omega} Q_{xy}(\omega + i\delta), \quad (4.2)$$

$$Q_{xy}(i\nu_m) = \frac{1}{\Omega\beta} \sum_{\mathbf{k}, n} \text{tr}[J_x(\mathbf{k})G(\mathbf{k}, i(\omega_n + \nu_m))J_y(\mathbf{k})G(\mathbf{k}, i\omega_n)], \quad (4.3)$$

with the current operator  $(i, j) = (x, y)$

$$J_i(\mathbf{k}) = \frac{\partial H(\mathbf{k})}{\partial k_i} = \frac{\partial \epsilon(\mathbf{k})}{\partial k_i} + V \frac{\partial_\alpha(\mathbf{k})}{\partial k_i} \sigma^\alpha \quad (4.4)$$

and  $G(\mathbf{k}, i\omega_n)$  the Matsubara Green function. From Eqs. (4.2) and (4.4), the Hall conductivity can be calculated straightforwardly, with the resulting  $\sigma_{xy}$  given by

$$\sigma_{xy} = \frac{1}{2\Omega} \sum_{\mathbf{k}} \frac{\partial \hat{d}_\alpha(\mathbf{k})}{\partial k_x} \frac{\partial \hat{d}_\beta(\mathbf{k})}{\partial k_y} \hat{d}_\gamma \epsilon^{\alpha\beta\gamma} (n_+ - n_-)(\mathbf{k}), \quad (4.5)$$

where  $\hat{d}_\alpha(\mathbf{k}) = d_\alpha(\mathbf{k})/d(\mathbf{k})$  is the unit vector along the direction of  $d_\alpha(\mathbf{k})$ .  $\hat{d}_\alpha(\mathbf{k})$  is singular if  $d(\mathbf{k}) = \sqrt{d_\alpha(\mathbf{k})d^\alpha(\mathbf{k})}$  vanishes for some  $\mathbf{k}$ . However, here and below we are always interested in the insulating models, in which a full gap opens between the two bands  $E_+(\mathbf{k})$  and  $E_-(\mathbf{k})$ ; thus  $E_+(\mathbf{k}) - E_-(\mathbf{k}) = 2Vd(\mathbf{k})$ , for all  $\mathbf{k}$ . The gap opening condition is written explicitly as

$$\min_{\mathbf{k} \in BZ} E_+(\mathbf{k}) > \max_{\mathbf{k} \in BZ} E_-(\mathbf{k}). \quad (4.6)$$

In this case, the system becomes a bulk insulator when the chemical potential lies inside the gap, which implies  $n(\mathbf{k}) \equiv 1$  and  $n_+(\mathbf{k}) \equiv 0$  for all  $\mathbf{k}$  at zero temperature. Under such condition and taking the thermodynamic limit, the Hall conductivity (4.5) can be simplified to

$$\sigma_x^y = -\frac{1}{4\pi^2} \int \int_{FBZ} dk_x dk_y \hat{\mathbf{d}} \cdot \partial_x \hat{\mathbf{d}} \times \partial_y \hat{\mathbf{d}}, \quad (4.7)$$

which is a topological invariant defined on the first Brillouin zone, independent of the details of the band structure parameters. Considering  $\hat{\mathbf{d}} : T^2 \rightarrow S^2$  as a mapping from the Brillouin zone to the unit sphere, the integrand is the Jacobian of this mapping. Thus the integration over it gives the total area of the image of the Brillouin zone on  $S^2$ , which is a topological winding number that is quantized. A schematic picture of a typical  $\hat{\mathbf{d}}$  configuration (a

half of Skyrmion, called also a meron) is shown in Fig. 4.2. Henceforth, the quantization of the conductivity in this system can be understood as a Berry phase in  $\mathbf{k}$  space, similar to the quantum Hall effect, with the Skyrmion winding number related to the quantization of the current. The universal spin conductivity obtained in this system is  $2e^2/h$ .

### 4.3 Conclusions

Either adding the spin degree of freedom to conventional charge-based electronic devices or using the spin alone has the potential advantages of non-volatility, increased data processing speed, decreased electric power consumption, and increased integration densities compared with conventional semiconductor devices. To successfully incorporate spins into existing semiconductor technology, one has to resolve technical issues such as efficient injection, transport, control and manipulation, and detection of spin polarization as well as spin-polarized currents [35]. There are numerous experimental challenges to overcome, as well as theoretical insight to be provided. But a spin-based electronics seems possible in the near future.

Future devices based on quantum spin-Hall effect will have the advantage that there is no magnetic field required. The spin current can flow without dissipation in quantum spin-Hall systems, which will increase a lot the efficiency of the data storage and of the computational time in the spintronic-based computers.

Cheap, easy to produce and feasible new materials which can host the quantum spin-Hall effect are requirements in order to have a large-scale industry based on spintronics.

Interesting enough, a topic with numerous possible applications, also poses insightful fundamental questions. The quantum spin Hall state is a novel topological state of matter, in the same way as the quantum Hall effect is. A lot of work still needs to be done before we can completely understand the properties of these systems.

# Bibliography

- [1] Shuichi Murakami, Naoto Nagaosa and Shou-Cheng Zhang. *Science*, **301**(5638):1348–1351, 2003.
- [2] Jairo Sinova, Dimitrie Culcer, Q. Niu, N. A. Sinitsyn, T. Jungwirth and A. H. MacDonald. *Phys. Rev. Lett.*, **92**(12):126603, Mar 2004.
- [3] Markus König, Steffen Wiedmann, Christoph Brune, Andreas Roth, Hartmut Buhmann, Laurens W. Molenkamp, Xiao-Liang Qi and Shou-Cheng Zhang. *Science*, **318**(5851):766–770, 2007.
- [4] K. v. Klitzing, G. Dorda and M. Pepper. *Phys. Rev. Lett.*, **45**(6):494–497, Aug 1980.
- [5] D. C. Tsui, H. L. Stormer and A. C. Gossard. *Phys. Rev. Lett.*, **48**(22):1559–1562, May 1982.
- [6] C. L. Kane and Matthew P. A. Fisher. *Phys. Rev. B*, **46**(11):7268–7271, Sep 1992.
- [7] J. E. Hirsch. *Phys. Rev. Lett.*, **83**(9):1834–1837, Aug 1999.
- [8] V.I. Perel M.I. Dyakonov. *Sov. Phys. JETP*, page 467, 1971.
- [9] Y. K. Kato, R. C. Myers, A. C. Gossard and D. D. Awschalom. *Science*, **306**(5703):1910–1913, 2004.
- [10] R. C. Kato Y. K. Lau W. H. Gossard A. C. Awschalom D. D. Sih, V. Myers. *Nature Physics*, **1**:31–35, 2005.
- [11] J. Wunderlich, B. Kaestner, J. Sinova and T. Jungwirth. *Physical Review Letters*, **94**(4):047204, 2005.
- [12] Jairo Sinova, T. Jungwirth, J. Kučera and A. H. MacDonald. *Phys. Rev. B*, **67**(23):235203, Jun 2003.

- [13] T. Jungwirth, Qian Niu and A. H. MacDonald. *Phys. Rev. Lett.*, **88**(20):207208, May 2002.
- [14] Jun-ichiro Inoue, Gerrit E. W. Bauer and Laurens W. Molenkamp. *Phys. Rev. B*, **70**(4):041303, Jul 2004.
- [15] E. G. Mishchenko, A. V. Shytov and B. I. Halperin. *Phys. Rev. Lett.*, **93**(22):226602, Nov 2004.
- [16] Emmanuel I. Rashba. *Phys. Rev. B*, **70**(20):201309, Nov 2004.
- [17] Olga V. Dimitrova. *Physical Review B (Condensed Matter and Materials Physics)*, **71**(24):245327, 2005.
- [18] Oleg Chalaev and Daniel Loss. *Physical Review B (Condensed Matter and Materials Physics)*, **71**(24):245318, 2005.
- [19] P. L. Krotkov and S. Das Sarma. *Physical Review B (Condensed Matter and Materials Physics)*, **73**(19):195307, 2006.
- [20] J. M. Luttinger. *Phys. Rev.*, **102**(4):1030–1041, May 1956.
- [21] M. V. Berry. *Proceedings of the Royal Society of London. Series A, Mathematical and Physical Sciences (1934-1990)*, **392**:45–57, 1984.
- [22] P. Prange and S.M. Girvin. *The Quantum Hall Effect*. Springer, Berlin, 1997.
- [23] J.D. Jackson. *Classical Electrodynamics*. Wiley, New York, 1998.
- [24] Andrei Bernevig, Taylor L. Hughes and Shou-Cheng Zhang. *Science*, **314**, 2006.
- [25] A. Zee. *Phys. Rev. A*, **38**(1):1–6, Jul 1988.
- [26] D. J. Thouless, M. Kohmoto, M. P. Nightingale and M. den Nijs. *Phys. Rev. Lett.*, **49**(6):405–408, Aug 1982.
- [27] P. R. Hammar, B. R. Bennett, M. J. Yang and Mark Johnson. *Phys. Rev. Lett.*, **83**(1):203–206, Jul 1999.
- [28] G. Schmidt, D. Ferrand, L. W. Molenkamp, A. T. Filip and B. J. van Wees. *Phys. Rev. B*, **62**(8):R4790–R4793, Aug 2000.
- [29] Shuichi Murakami, Naoto Nagosa and Shou-Cheng Zhang. *Phys. Rev. B*, **69**(23):235206, Jun 2004.

- [30] C.L. Kane and E.J. Mele. *Phys. Rev. Lett*, **95**:226801, 2005.
- [31] B. Andrei Bernevig and Shou-Cheng Zhang. *Physical Review Letters*, **96**(10):106802, 2006.
- [32] Congjun Wu, B. Andrei Bernevig and Shou-Cheng Zhang. *Physical Review Letters*, **96**(10):106401, 2006.
- [33] Cenke Xu and J. E. Moore. *Physical Review B (Condensed Matter and Materials Physics)*, **73**(4):045322, 2006.
- [34] Xiao-Liang Qi, Yong-Shi Wu and Shou-Cheng Zhang. *Physical Review B (Condensed Matter and Materials Physics)*, **74**(8):085308, 2006.
- [35] S. A. Wolf, D. D. Awschalom, R. A. Buhrman, J. M. Daughton, S. von Molnar, M. L. Roukes, A. Y. Chtchelkanova and D. M. Treger. *Science*, **294**(5546):1488–1495, 2001.



# Appendix A

## $\mathbf{k} \cdot \mathbf{p}$ approximation for semiconductors

Semiconductors band structure can be described using the  $\mathbf{k} \cdot \mathbf{p}$  method (also named effective mass approximation). This is a perturbative method to calculate the eigenfunctions (and the corresponding eigenenergies) at a certain momentum by knowing the eigenfunctions and eigenenergies at zero value of momentum.

The electrons in a periodic crystal are described by the Bloch wavefunctions

$$\Psi_{n\mathbf{k}}(\mathbf{x}) = u_{n\mathbf{k}}(\mathbf{x})e^{i\mathbf{k}\mathbf{x}}, \quad (\text{A.1})$$

where  $n$  labels the bands and  $u_{n\mathbf{k}}(\mathbf{x} + \mathbf{a}_i) = u_{n\mathbf{k}}(\mathbf{x})$  is a function with periodicity of the crystal. The atomic-like wavefunctions are  $u_{m0}(\mathbf{x})$  and therefore the wavefunctions at momentum  $\mathbf{k}$  are exactly expressed as linear combinations

$$u_{n\mathbf{k}}(\mathbf{x}) = \sum_{n'} A_{nn'\mathbf{k}} u_{n'0}(\mathbf{x}). \quad (\text{A.2})$$

We replace the Eq.(A.1) in Schrodinger equation

$$\left[ \frac{\hat{\mathbf{p}}^2}{2m} + V(\mathbf{x}) \right] \Psi_{n\mathbf{k}}(\mathbf{x}) = \varepsilon_{n\mathbf{k}} \Psi_{n\mathbf{k}}(\mathbf{x}). \quad (\text{A.3})$$

The action of the momentum operator on wavefunction (A.1) results in

$$e^{i\mathbf{k}\mathbf{x}} \left( -\frac{\hbar^2}{2m} \Delta + \frac{\hbar\mathbf{k}}{m} \cdot \frac{\hbar}{i} \nabla + \frac{\hbar^2 k^2}{2m} \right) u_{n'0}(\mathbf{x}), \quad (\text{A.4})$$

and we also know the solutions for eigenvalue problem for the  $k = 0$  :  $\left[ \frac{\hat{\mathbf{p}}^2}{2m} + V(\mathbf{x}) \right] u_{n'0}(\mathbf{x}) = \varepsilon_{n'0} u_{n'0}(\mathbf{x})$ . Thus we obtain a Schrödinger-like equation for the coefficients  $A_{nn'\mathbf{k}}$

$$\left( \varepsilon_{n'0} + \frac{\hbar^2 k^2}{2m} \right) A_{nn'\mathbf{k}} + \frac{\hbar \mathbf{k}}{m} \cdot \sum_l \mathbf{P}_{n'l} A_{nl\mathbf{k}} = \varepsilon_{n\mathbf{k}} A_{nn'\mathbf{k}}, \quad (\text{A.5})$$

where  $P_{n'l} = \int_{\text{unitcell}} d^3x u_{n'0}^*(\mathbf{x}) \frac{\hbar}{i} \nabla u_{l0}(\mathbf{x})$  is the effective momentum operator. The atomic wavefunctions are orthonormal.

The approximation consists in considering the  $\frac{\hbar}{m} \mathbf{k} \cdot \mathbf{p}$  term in equation A.5 as a perturbation. This assumption holds for small momenta  $k \ll |\mathbf{G}|$ , with  $\mathbf{G}$  the reciprocal lattice vector. In materials with inversion symmetry, the diagonal components of the momentum operator are zero which implies that the first correction to the energy is also zero. To see this we use the definition of  $\mathbf{P}$

$$P_{nn} = \frac{\hbar}{i} \int d^3x u_{n0}^*(\mathbf{x}) \frac{\partial u_{n0}}{\partial \mathbf{x}}(\mathbf{x}), \quad (\text{A.6})$$

which upon spatial inversion  $\mathbf{x} \rightarrow -\mathbf{x}$  becomes

$$- \frac{\hbar}{i} \int d^3x u_{n0}^*(-\mathbf{x}) \frac{\partial u_{n0}}{\partial \mathbf{x}}(-\mathbf{x}). \quad (\text{A.7})$$

We use that the Wannier wavefunctions are inversion symmetric, namely that  $u_{n0}(-\mathbf{x}) = \pm u_{n0}(\mathbf{x})$ , to find that Eq.(A.6) becomes

$$- \frac{\hbar}{i} \int d^3x u_{n0}^*(\mathbf{x}) \frac{\partial u_{n0}}{\partial \mathbf{x}}(\mathbf{x}) = -P_{nn} = 0, \quad (\text{A.8})$$

which concludes the proof.

The first order correction to the wavefunction is

$$A_{nn'\mathbf{k}}^{(1)} = \frac{\hbar \mathbf{k}}{m} \cdot \frac{P_{nn'}}{\varepsilon_{n0} - \varepsilon_{n'0}}. \quad (\text{A.9})$$

The second order correction to the energy is non-zero and the total energy up to the second order correction reads

$$\varepsilon_{n\mathbf{k}} \simeq \varepsilon_{n0} + \frac{\hbar^2 k^2}{2m} + \frac{\hbar^2 k^\alpha k^\beta}{m^2} \sum_{n' \neq n} \frac{P_{nn'}^\alpha P_{nn'}^\beta}{\varepsilon_{n0} - \varepsilon_{n'0}} \quad (\text{A.10})$$

$$\equiv \varepsilon_{n0} + D_{nn}^{\alpha\beta} k^\alpha k^\beta, \quad (\text{A.11})$$

where

$$D_{ln}^{\alpha\beta} = \hbar^2 \left( \frac{\delta^{\alpha\beta} \delta_{ln}}{2m} + \frac{1}{m^2} \sum_{n' \neq n} \frac{P_{nn'}^\alpha P_{nn'}^\beta}{\varepsilon_{n0} - \varepsilon_{n'0}} \right) \quad (\text{A.12})$$

is the inverse effective mass tensor. Above we have assumed that bands are not degenerate at the  $\Gamma$ -point. Therefore only the diagonal matrix elements of the tensor were sufficient. But often the bands are degenerate at the  $\mathbf{k} = 0$  point due to symmetry reasons. Then the full tensor is needed. The second order correction to energy is now an operator, playing the role of effective Hamiltonian

$$(\varepsilon_{\mathbf{k}})_{ln} = \varepsilon_{n0} \delta_{ln} + D_{ln}^{\alpha\beta} k^\alpha k^\beta. \quad (\text{A.13})$$

To find the energies for  $\mathbf{k} \neq 0$  one has to diagonalize the matrix. Away from the  $\Gamma$ -point the degeneracy is partially lifted. The usual difficulty resides in finding the matrix elements  $P_{nn'}^\alpha$  in expression (A.12). Using symmetry reasons is the common way to deal with it, providing satisfactory approximations. For example, in a cubic environment, these matrix elements are linear combinations of the spherical harmonics.

# Appendix B

## Integrating the equation of motions for holes in the Abelian approximation

The set of coupled equations of motion (3.17) can be analytically integrated. Since the equations for the momenta  $k_i$  are trivial, we only focus here on finding the solutions for  $x_i$ .

The equations to solve are

$$\frac{dx_i}{dt} = \frac{\hbar k_i}{m_\lambda} + F_{ij} \frac{dk_j}{dt}. \quad (\text{B.1})$$

We know the solutions for  $k$ -s to be

$$k_i(t) = k_i(0) + \frac{eE_i}{\hbar}t, \quad (\text{B.2})$$

and the field strength tensor  $F_{ij} = \varepsilon_{ijl}\lambda\frac{k_l}{k^3}$ . Hence the equations (B.1) read

$$\frac{dx_i}{dt} = \frac{\hbar k_i}{m_\lambda} + \lambda\frac{e}{\hbar}\varepsilon_{ijl}\frac{k_l}{k^3}E_j. \quad (\text{B.3})$$

We chose the electric to be parallel to the  $z$  axis. Thus the  $x$  and  $y$  components of momenta will be constant and given by the initial conditions, and the third one will be time-dependent:

$$k_1(t) \equiv k_1(t=0) = k_{10} \quad (\text{B.4})$$

$$k_2(t) \equiv k_2(t=0) = k_{20} \quad (\text{B.5})$$

$$k_3(t) = k_{30} + \frac{e}{\hbar}E_z \cdot t. \quad (\text{B.6})$$

Thus the total momenta cubed is  $k^3 = [k_{10}^2 + k_{20}^2 + (k_{30} + eE_z t/\hbar)^2]^{3/2}$ . The equations for the positions become

$$dx_i = \frac{\hbar}{m_\lambda} k_{i0} dt + \frac{e}{\hbar} E_i t dt + \lambda \frac{e}{\hbar} E_j \varepsilon_{ijl} \frac{k_l + \frac{e}{\hbar} E_i}{[k_{10}^2 + k_{20}^2 + (k_{30} + eE_z t/\hbar)^2]^{3/2}} dt$$

We integrate the latter equation between 0 to  $t$  to get

$$x_i(t) - x_i(0) = \frac{\hbar}{m_\lambda} k_{i0} t + \frac{e}{2\hbar} E_i t^2 + \lambda \frac{e}{\hbar} E_j \varepsilon_{ijl} \int_0^t dt' \frac{k_l + eE_i t'/\hbar}{[k_{10}^2 + k_{20}^2 + (k_{30} + eE_z t'/\hbar)^2]^{3/2}}$$

The last step now is to perform the integral in the last term. To make the procedure simpler we replace the only non-zero component of the electric field,  $E_1 = E_2 = 0$ ,  $E_3 \equiv E_z \neq 0$  and identifying the Cartesian components  $1 \equiv x$ ,  $2 \equiv y$  and  $3 \equiv z$ . E.g., the first component is

$$x_1 \equiv x(t) = x_0 + \frac{\hbar k_{10}}{2m_\lambda} t + \lambda \frac{e}{\hbar} \varepsilon_{132} E_z \int_0^t dt' \frac{k_{20}}{[k_{10}^2 + k_{20}^2 + (k_{30} + eE_z t'/\hbar)^2]^{3/2}} \quad (\text{B.7})$$

In consequence the integral becomes trivial and the results read

$$\begin{aligned} x(t) &= x_0 + \frac{\hbar k_{x0}}{m_\lambda} t - \frac{\lambda k_{y0}}{k_{x0}^2 + k_{y0}^2} \frac{eE_z t/\hbar + k_{z0}}{\sqrt{k_{x0}^2 + k_{y0}^2 + (eE_z t/\hbar + k_{z0})^2}}, \\ y(t) &= y_0 + \frac{\hbar k_{y0}}{m_\lambda} t + \frac{\lambda k_{x0}}{k_{x0}^2 + k_{y0}^2} \frac{eE_z t/\hbar + k_{z0}}{\sqrt{k_{x0}^2 + k_{y0}^2 + (eE_z t/\hbar + k_{z0})^2}}, \\ z(t) &= z_0 + \frac{\hbar k_{z0}}{m_\lambda} + \frac{eE_z}{2m_\lambda} t^2. \end{aligned}$$

# Appendix C

## Acknowledgements

I would like to thank my advisor Maxim Mostovoy for his guidance as well as for his patience during my many tribulations regarding the topic of my Master's thesis. I am very grateful for his encouragement and support to attend scientific meetings, such as Physics@Veldoven, Driebergen Spring School in Statistical and Condensed Matter Theory and others. Maxim encourages young people to pursue their own research interests, and to learn as much as possible. For those reasons I am indeed grateful, as I certainly am for all his help and the knowledge that he has shared with his students. During this last year I have indeed learned a lot.

Thanks to Sergey Artyukhin who is enthusiastically interested in any physics problem. During useful discussions with him and with Andrei Berceanu I came to understand a lot about the physics underlying the spin-Hall effect.

I would like to thank Elisabetta Pallante for accepting to evaluate this thesis. To Michiel van der Vegte I am indebted for the collaboration during the first months of my research, the “spin ladder” period, as a continuation to our previous successes on vanadium dioxide.

Wioletta Ruszel, Siebren Reker and Thomas de la Cour Jansen have helped me to keep good humor during less easy times as well as in good ones. It was great to have Elena Diaz-Garcia as a guest in the Institute, too bad that it was for only three months.

The secretaries of the Institute of Theoretical Physics, Iris de Roo-Kwant and Sietske Rob have always been very helpful and nice.

Last but not least, I am indebted to the Zernike Institute for Advanced Materials and the University of Groningen for supporting the Top Master Programme in Nanoscience.